induced by a choline-methionine-deficient diet, serotonin-deficient tryptophan hydroxylase knock-out mice showed reduced hepatocellular injury and less severe inflammation (9). Liver steatosis induced by lymphocytic choriomeningitis virus infection is also serotonin-dependent (10), suggesting the involvement of serotonin in liver steatosis. Meanwhile, L-kynurenine is synthesized by indoleamine 2,3-dioxygenase (IDO) from L-tryptophan, which accounts for ~90% of tryptophan catabolism (4). L-Leucine is a branched amino acid and is involved in liver protein synthesis. L-Leucine deprivation induces liver steatosis in Gcn2 knock-out mice (15), whereas L-leucine supplementation reduced hepatic steatosis induced by high fat diet (16), suggesting a possible protective role of L-leucine against liver steatosis.

The mammalian target of rapamycin (mTOR) is a serine/threonine kinase and forms protein complexes that induce lipogenic gene expression (17). mTOR is activated in the livers of obese rats fed a high fat and high sucrose diet (18). The mTOR complex is important in the stimulation of lipogenesis in the liver (19), and the mTOR kinase inhibitor rapamycin reduces hepatic steatosis induced by a high fat diet (20). mTOR is also a master regulator of autophagy (21, 22), which is the process of degradation of intracellular components and distribution of nutrients under starving conditions. Upon food intake, amino acids and insulin inhibit autophagy through the mTOR and/or AKT-dependent pathways (23). Importantly, hepatic autophagy induces the breakdown of lipids stored in lipid droplets and regulates the lipid content in the liver (24, 25).

In the present study, we investigate the effects of L-tryptophan in hepatic steatosis. Our results suggest that L-tryptophan exacerbates hepatic steatosis induced by a high fat and high fructose diet (HFHFD) through serotonin and the activation of mTOR.

EXPERIMENTAL PROCEDURES

Animal Experiments—The experiments were conducted in accordance with the institutional guideline of Gifu University. Male wild-type C57BL/6J mice at 4 weeks of age were obtained from Japan SLC (Shizuoka, Japan). The mice were kept on a 12-h day/night cycle with free access to food and water. Hepatic steatosis was induced by feeding the animals HFHFD (a high fat diet (62.2% of calories from fat) (Oriental Yeast, Tokyo, Japan; HFD-60) and drinking water containing 30% fructose (Wako, Osaka, Japan)) for 8 weeks. Control mice were fed a normal diet (12.6% of calories from fat) (CLEA Japan, Tokyo, Japan; CE-2) with plain water. L-Tryptophan or L-leucine (Sigma-Aldrich) was administered in the drinking water at a concentration of 0.25% (w/v) (L-tryptophan) and 1% (L-leucine), respectively, at a dose of ~400 and 1600 mg/kg/day. Control animals were treated with bovine serum albumin (BSA) (Wako, Osaka, Japan) in the drinking water at a concentration of 0.25%. At the end of the study period, the animals were deprived of food for 18 h, and the drinking water was changed to plain water without fructose, L-tryptophan, or L-leucine. After recording body weight, the mice were anesthetized and humanely killed by withdrawal of blood. The liver was immediately removed and washed in ice-cold phosphate-buffered saline (PBS). Subsequently, weight measurements of liver were taken, and a part of the dissected liver tissue was frozen in liquid nitrogen. Serum alanine aminotransaminase was measured using an automatic analyzer (JEOL Ltd., Tokyo, Japan; BM2250).

Cell Culture and Treatments—Male wild-type C57BL/6J mice (8–12 weeks old) were anesthetized, and then hepatocytes were isolated by a nonrecirculating *in situ* collagenase perfusion of livers cannulating through the inferior vena cava as described previously (26) with minor modifications. Livers were first perfused *in situ* with 0.5 mM EGTA containing calcium-free salt solution, followed by perfusion with solution containing collagenase (0.65 mg/ml) (Wako). The livers were then gently minced on a Petri dish and filtered with nylon mesh (Tokyo Screen, Tokyo, Japan; N-No.270T). Hepatocytes were washed three times with Hanks' balanced salt solution (HBSS). Cell viability was consistently >90%, as determined by trypan blue exclusion. Cells were plated on 6-well plates (1×10^6 cells/well) coated with rat tail collagen type I (BD Biosciences; BioCoat) in Waymouth medium (Invitrogen) containing 10% fetal bovine serum supplemented with penicillin and streptomycin (Invitrogen) for 4 h. Hc hepatocytes (normal human fetal hepatocytes) and cell culture medium (CS-C complete) was obtained from Applied Cell Biology Research Institute and Cell Systems, respectively. Hc hepatocytes were cultured in CS-C complete medium supplemented with penicillin and streptomycin and maintained at 37 °C in a 5% CO_2 atmosphere. Cells were plated on 6-well plates (1×10^6 cells/well) and were incubated in the medium for 24 h. Primary cultured mouse hepatocytes and Hc hepatocytes were then washed twice with PBS, and the medium was changed to serum-free RPMI 1640 containing 0.5% BSA and the antibiotics. After a 1-h incubation, the cells were treated with or without 100 μM serotonin (Sigma-Aldrich) and/or fatty acid mixture (100 μM linoleic acid and 100 μM oleic acid) (Sigma-Aldrich; L9655) for 2 h for protein extraction and 18 h for Oil Red O staining and triglyceride measurement. When necessary, the cells were pretreated with 100 nM rapamycin (Sigma-Aldrich) dissolved in DMSO for 30 min before treatment with serotonin and/or fatty acids. For induction of autophagy in Hc hepatocytes, cells were washed twice with PBS, and the medium was changed to HBSS with or without rapamycin. After a 0.5-h incubation, the cells were treated with or without serotonin and incubated for an additional 3 h. For control, the cells were cultured in RPMI1640 medium containing 10% FBS.

Histological Analysis—The livers were fixed with 10% formalin, and paraffin blocks were sectioned and stained with hematoxylin and eosin (H&E). Collagen deposition was stained with Sirius Red (saturated picric acid containing 0.1% DirectRed 80 and 0.1% FastGreen FCF) as reported previously (27). For frozen liver sections, the fixed livers were soaked in 15% sucrose in PBS for 12 h following with 30% sucrose for 24 h at 4 °C under constant agitation and were then embedded in OTC compound. For 4-hydroxy-2-nonenal (HNE) staining, the frozen liver sections were cut at a thickness of 5 μm with a cryostat and stained with anti-HNE antibody (Alpha Diagnostic International; HNE11-S).

Oil Red O Staining—For lipid droplet staining, the frozen liver sections were cut at a thickness of 5 μm using a cryostat

and were subsequently stained with Oil Red O (Muto Pure Chemicals, Tokyo, Japan) working solution. Hematoxylin was used for counterstaining. For cells, the Hc hepatocytes were fixed with 10% formalin and then stained with Oil Red O.

Measurement of Triglyceride—Triglyceride content in the serum, liver tissue, and cells was measured using a triglyceride E-test kit (Wako). For liver tissues, the frozen liver tissues were homogenized in PBS, and methanol was added to the lysate. For cells, the Hc hepatocytes were washed with PBS and scraped with methanol. The lipids were extracted by the Bligh and Dyer method.

Western Blot—For the preparation of total cell proteins, cells or frozen liver tissues were sonicated in radioimmunoprecipitation assay buffer (50 mM Tris-HCl, pH 7.5, 150 mM NaCl, 10 mM EGTA, 1% Triton-X, 0.1% SDS) containing protease inhibitors and phosphatase inhibitors (Roche Applied Science; PhosSTOP phosphatase inhibitor mixture and Complete protease inhibitor mixture tablets). The proteins were separated by SDS-PAGE and were electrophoretically transferred onto nitrocellulose membrane. The membranes were first incubated with the primary antibodies, anti-HNE, phospho-mTOR (Ser^{2448}) (Cell Signaling Technology; catalog no. 2971), mTOR (Cell Signaling; catalog no. 2972), phospho-p70S6K (Thr^{389}) (Cell Signaling; catalog no. 9234), p70S6K (Cell Signaling; catalog no. 2708), phospho-AKT (Ser^{473}) (Cell Signaling; catalog no. 9271), AKT (Cell Signaling; catalog no. 9272), phospho-AMP-activated protein kinase α (AMPKα) (Thr^{172}) (Cell Signaling; catalog no. 2531), AMPKα (Cell Signaling; catalog no. 2603), p62 (MBL; PM045), and glyceraldehyde 3-phosphate dehydrogenase (GAPDH) (Cell Signaling; catalog no. 2118) antibodies. Then the membranes were incubated with the horseradish peroxidase (HRP)-coupled secondary antibodies (Santa Cruz Biotechnology, Inc., Santa Cruz, CA). Detection was performed with ImmunoStar LD (Wako), and the protein bands were quantified by densitometry using the ImageJ program (National Institutes of Health, Bethesda, MD).

Quantitative Real-time RT-PCR—Extracted RNA from the liver was reverse-transcribed by a high capacity cDNA reverse transcription kit (Applied Biosystems), and quantitative real-time PCR was performed using SYBR premix Ex Taq (Takara, Shiga, Japan) with ABI Prism 7000 (Applied Biosystems). The changes were normalized based on 18 S rRNA. PCR primer sequences were listed as follows: transforming growth factor (TGF)-β1, GTGGAAATCAACGGGATCAG (forward) and ACTTCCAACCCAGGTCCTTC (reverse); collagen α1(I), TAGGCCATTGTGTATGCAGC (forward) and ACATGTTCAGCTTTGTGGACC (reverse); 18 S, AGTCCCTGCCCTTTGTACACA (forward) and CGATCCGAGGGCCTCACTA (reverse).

Hydroxyproline Measurement—Hydroxyproline was measured for assessment of collagen content. The extracted liver protein was hydrolyzed in 6 M HCl (100 °C, 24 h). The samples were neutralized with LiOH, and hydroxyproline content was measured using a high performance liquid chromatographic analyzer (Jasco, Hitachi, and Shimazu).

Recombinant Adenoviruses—The recombinant replication-deficient adenoviruses Ad5IDO and Ad5AADC, expressing IDO and AADC, respectively, were constructed by the AdEasy™ adenoviral vector system (Stratagene) as described previously (28). Briefly, the full length of mouse IDO and AADC cDNA was amplified by PCR with the following primers: IDO, ATAGGTACCGCCGCCATGGCACTCAGTAAAATATCTCCTACAGAAGGTTC (forward) and ATACTCGAGCTAAGGCCAACTCAGAAGAGCTTTCTCGGTTGTATCTTT (reverse); AADC, ATAGGTACCGCCGCCATGGATTCCCGTGAATTCCGGAGGAGAGGCAAGGA (forward) and ATACTCGAGTCATTCTTTCTCTGCCCTCAGCACACTGCTTGCTAG (reverse). The cDNA fragment was subcloned into pAdTrack-CMV adenoviral vector. The plasmid DNA was prepared by the alkaline lysis method and transfected into BJ5183-AD-1 electroporation-competent cells. The virus was grown in 293 cells and purified by banding twice on CsCl gradients and then dialyzed and stored at −20 °C. Mice were infected with the adenoviruses (5×10^8 pfu/mouse) by intravenous injection 7 days before sacrifice. Gene expressions by the adenovirus vectors were preferentially observed in the liver (mainly in the hepatocytes) but not in the muscle and adipose tissue (data not shown), as reported previously (28, 29). The adenovirus Ad5GFP, which expresses green fluorescent protein, was used as infection control.

Measurement of L-Tryptophan, L-Kynurenine, and Serotonin—Serum L-tryptophan and L-kynurenine were measured by HPLC with a spectrophotometric detector (Tosoh, Tokyo, Japan; Tosoh ultraviolet-8000) or fluorescence spectrometric detector (Hitachi, Tokyo, Japan) as described in a previous report (30). Serum serotonin was measured by Serotonin FAST ELISA (DRG International, Marburg, Germany).

Statistical Analysis—The results shown are representative of at least three independent experiments. Data are expressed as mean ± S.D. from at least four independent experiments. Data between groups were analyzed by Student's *t* test. A value of $p < 0.05$ was considered statistically significant.

RESULTS

L-Tryptophan Exacerbates Hepatic Steatosis and Fibrosis—Hepatic steatosis was induced by HFHFD in mice. The HFHFD caused an increase in body weight (Fig. 1*A*) and induced hepatic steatosis (Fig. 1, *B* and *C*), whereas the body/liver weight ratio was decreased (Fig. 1*A*). To examine the effect of L-tryptophan on hepatic steatosis, mice fed with HFHFD were treated with L-tryptophan or BSA. To confirm the specific effect of L-tryptophan, L-leucine was used as a control amino acid. Although L-tryptophan alone did not induce hepatic steatosis, a combination of L-tryptophan and HFHFD exacerbated hepatic steatosis and reversed the reduction of the body/liver weight ratio (Fig. 1, *A–C*) without changing food and water intake, blood glucose, or serum triglyceride levels (data not shown). L-Tryptophan treatment with HFHFD significantly increased serum alanine aminotransaminase levels (Fig. 2*A*) and formation of reactive oxygen species (ROS) as assessed by expression of HNE-modified proteins (Fig. 2*B*). Although expression of fibrogenic gene collagen α1(I), but not TGF-β, was up-regulated in HFHFD-fed animals (Fig. 2*C*), L-tryptophan treatment further increased the expression of TGF-β and collagen α1(I) in the livers of mice treated with HFHFD (Fig. 2*C*).

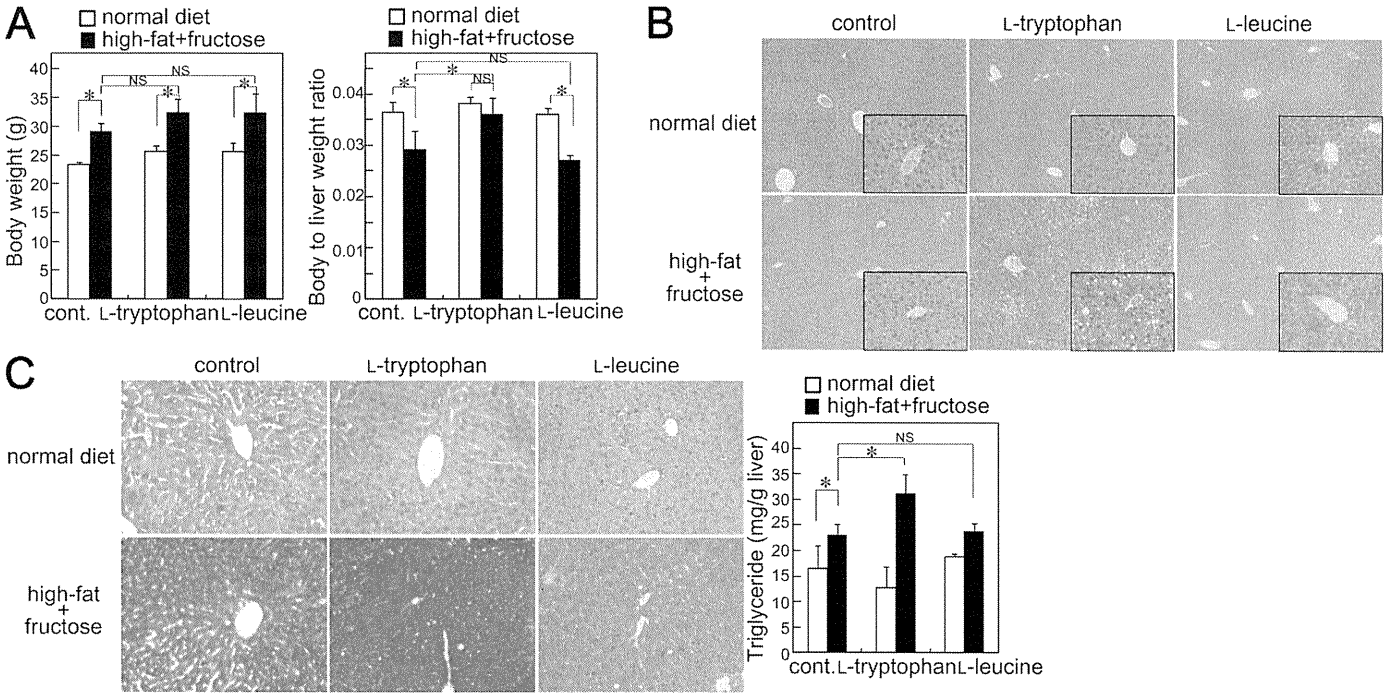

FIGURE 1. **L-Tryptophan exacerbates hepatic steatosis.** Mice were fed a normal diet or HFHFD supplemented with or without L-tryptophan or L-leucine for 8 weeks. The animals were humanely killed under fasting conditions (18 h of food deprivation). *A*, body weight (*left*) and liver weight were measured, and the body/liver weight ratio was calculated (*right*). *B*, liver sections were stained with H&E (original magnification, ×100 and ×400 (*insets*)). *C*, hepatic lipid content was assessed by Oil Red O staining (*left*; original magnification, ×200) and triglyceride measurement (*right*). Results shown are representative of at least three independent experiments. Data are means ± S.D. from at least four independent experiments. *, $p < 0.05$. *NS*, not significant.

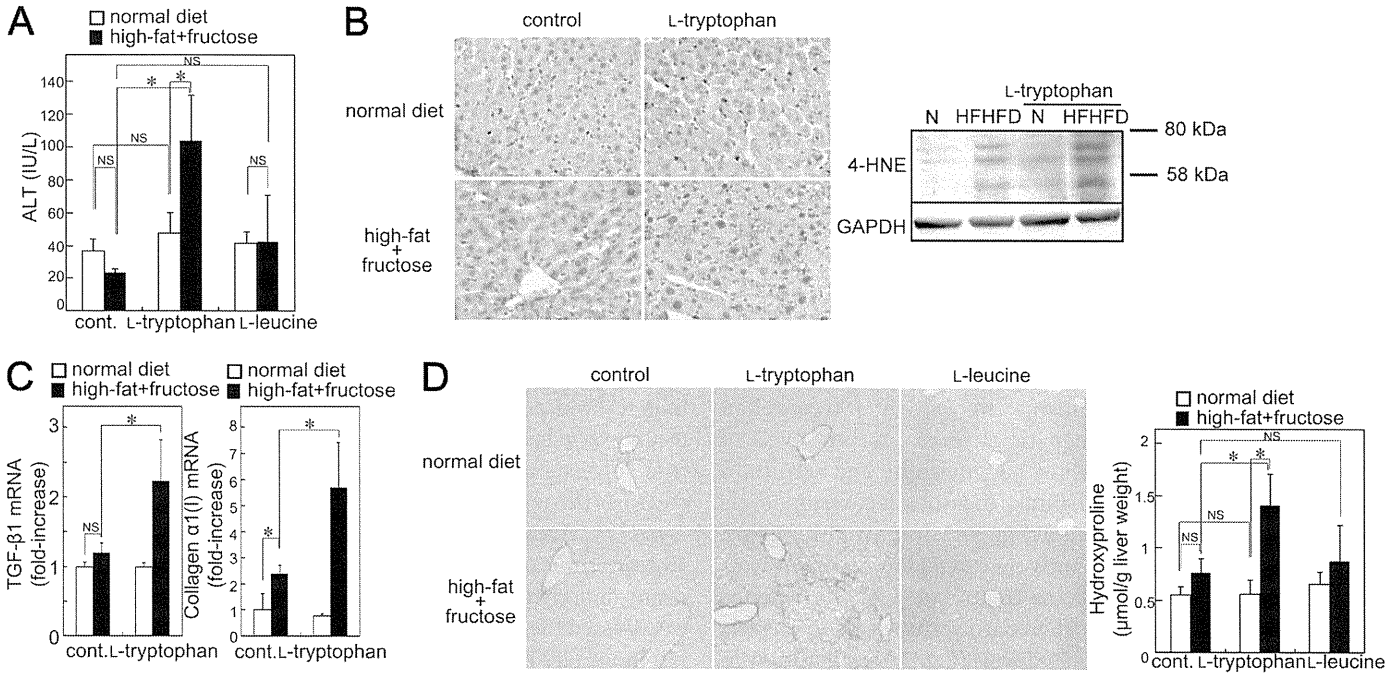

FIGURE 2. **L-Tryptophan induces hepatic fibrosis in steatotic liver.** Mice were fed a normal diet (*N*) or HFHFD supplemented with or without L-tryptophan or L-leucine for 8 weeks. *A*, serum alanine aminotransaminase levels were compared. *B*, expression of HNE-modified proteins in liver tissue was examined by immunohistochemistry (*left*; original magnification, ×400). Protein extracts from liver tissue were subjected to SDS-PAGE, and immunoblotting was performed with anti-HNE and GAPDH antibodies (*right*). *C*, mRNA levels of TGF-β1 and collagen α1(I) in liver tissue were determined by quantitative real-time RT-PCR. *D*, collagen deposition was assessed by Sirius Red staining (*left*; original magnification, ×200) and measurement of hydroxyproline content (*right*). Results shown are representative of at least three independent experiments. Data are means ± S.D. from at least four independent experiments. *, $p < 0.05$. *NS*, not significant.

Interestingly, although a combination of the L-tryptophan and HFHFD treatments induced liver fibrosis, neither treatment alone induced liver fibrosis (Fig. 2*D*). In contrast, L-leucine treatment did not enhance HFHFD-mediated steatosis, liver injury, and fibrosis (Fig. 2, *A* and *D*). These results suggest that the L-tryptophan increases hepatic steatosis, ROS

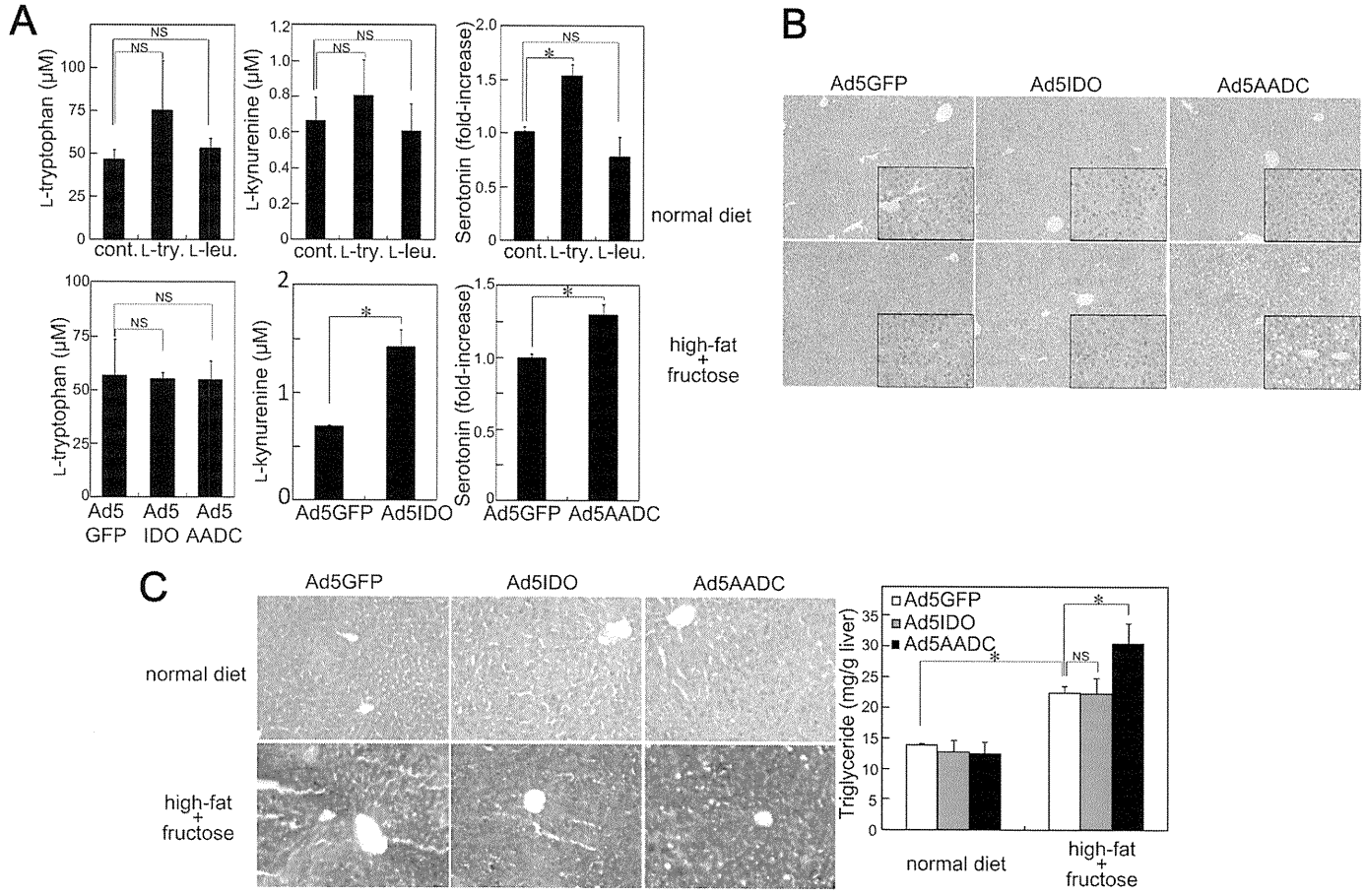

FIGURE 3. **Exogenous introduction of AADC aggravates hepatic steatosis.** *A*, mice were fed a normal diet supplemented with or without L-tryptophan or L-leucine for 8 weeks (*top panels*). Mice were infected with Ad5GFP, Ad5IDO, or Ad5AADC (5×10^8 pfu/mouse) and were humanely killed 7 days after the adenoviral infection (*bottom panels*). Serum L-tryptophan, L-kynurenine, and serotonin levels were measured. *B*, mice were fed with a normal diet or HFHFD for 8 weeks. The mice were infected with or without Ad5GFP, Ad5IDO, or Ad5AADC (5×10^8 pfu/mouse) at the end of 7-week period and were humanely killed on 7 days after the adenoviral infection under fasting conditions (18 h of food deprivation). Liver sections were stained with H&E (original magnification, ×100 and ×400 (insets)). *C*, hepatic lipid content was assessed by Oil Red O staining (*left*; original magnification, ×200) and triglyceride measurement (*right*). Results shown are representative of at least three independent experiments. Data are means ± S.D. from at least four independent experiments. *, $p < 0.05$. *NS*, not significant.

production, liver injury, and fibrosis induced by excessive fat and fructose intake.

Exogenous AADC or Serotonin Aggravates Hepatic Steatosis—To investigate the mechanisms by which L-tryptophan enhances HFHFD-induced hepatic steatosis, serum levels of L-tryptophan and its metabolites L-kynurenine and serotonin were measured. L-Tryptophan intake did not affect serum levels of L-tryptophan or L-kynurenine (Fig. 3*A*). Importantly, serum serotonin levels were significantly increased by treatment with L-tryptophan but not by L-leucine treatment (Fig. 3*A*). Adenoviral AADC introduction also increased serum serotonin levels without decreasing L-tryptophan levels (Fig. 3*A*) in addition to increased hepatic steatosis and triglyceride levels in HFHFD-fed animals (Fig. 3, *B* and *C*). Ad5IDO-infected mice with increased levels of serum L-kynurenine showed similar levels of lipid accumulation compared with control adenovirus-infected mice (Fig. 3*A*). This indicates synthesis of serotonin but not kynurenine as a crucial component of hepatic steatosis enhanced by L-tryptophan treatment. Subsequently, we investigated the effect of serotonin on lipid accumulation *in vitro* using primary cultured hepatocytes and Hc hepatocytes. The serotonin treatment in addition to fatty acid (linoleic acid and oleic acid) amplified the effects, such as accumulation of lipid droplets and increase of triglycerides, seen in fatty acid-treated cells (Fig. 4, *A* and *B*). In contrast, serotonin alone did not induce lipid accumulation. These results indicate that serotonin exacerbates lipid accumulation in hepatocytes. This further suggests that L-tryptophan treatment aggravates hepatic steatosis through serotonin.

mTOR Activation Is Crucial for L-Tryptophan-mediated Exacerbation of Hepatic Steatosis—To investigate the mechanisms underlying the effect of L-tryptophan on hepatic steatosis, we assessed the activation of mTOR, AKT, and AMPK, which are key molecules in the regulation of lipogenesis (17, 28). L-Tryptophan treatment induced phosphorylation of mTOR and p70S6K, a downstream target of mTOR in mouse livers under food-deprived conditions (Fig. 5*A* and supplemental Fig. 1*A*). In contrast, L-leucine treatment did not affect phosphorylation of mTOR or p70S6K. Although the HFHFD alone increased AKT and decreased AMPK phosphorylation, L-tryptophan or L-leucine treatment did not affect AKT or AMPK phosphorylation. Adenoviral AADC introduction also increased the phosphorylation of mTOR and p70S6K (Fig. 5*B* and supplemental Fig. 1*A*), suggesting that increased serotonin levels induce mTOR and p70S6K phos-

phorylation. Importantly, serotonin treatment increased mTOR and p70S6K phosphorylation in both primary cultured mouse hepatocytes and Hc hepatocytes (Fig. 6, *A* and *B*, and supplemental Fig. 1*B*). These results led to the hypothesis that mTOR activation contributes to the L-tryptophan/serotonin-mediated exacerbation of hepatic steatosis. Therefore, we investigated the role of serotonin-mediated mTOR activation by inhibiting mTOR activation using rapamycin, a potent inhibitor of mTOR. Rapamycin successfully inhibited the serotonin-mediated phosphorylation of mTOR and p70S6K (Fig. 6, *A* and *B*, and supplemental Fig. 1*B*) and lipid accumulation (Fig. 6, *C* and *D*). The requirement of mTOR activation in L-tryptophan/serotonin signaling for hepatic steatosis was also examined *in vivo*. Treatment with rapamycin significantly inhibited the phosphorylation of mTOR and p70S6K induction by L-tryptophan in mouse livers (supplemental Fig. 2*A*). Normal body weight increase following HFHFD was also diminished in rapamycin-treated mice (supplemental Fig. 2*B*) without change in the food or water intake (data not shown), as reported previously (20). Moreover, rapamycin treatment attenuated hepatic steatosis (supplemental Fig. 2, *C* and *D*), levels of alanine aminotransaminase (supplemental Fig. 2*E*), hepatic expression of HNE-modified proteins (supplemental Fig. 2*F*), and hepatic hydroxyproline content (supplemental Fig. 2*G*) in HFHFD and L-tryptophan-treated mice. These results suggest requirement of mTOR activation for the exacerbation of hepatic steatosis, liver damage, ROS formation, and liver fibrosis in the HFHFD- and L-tryptophan-treated animals.

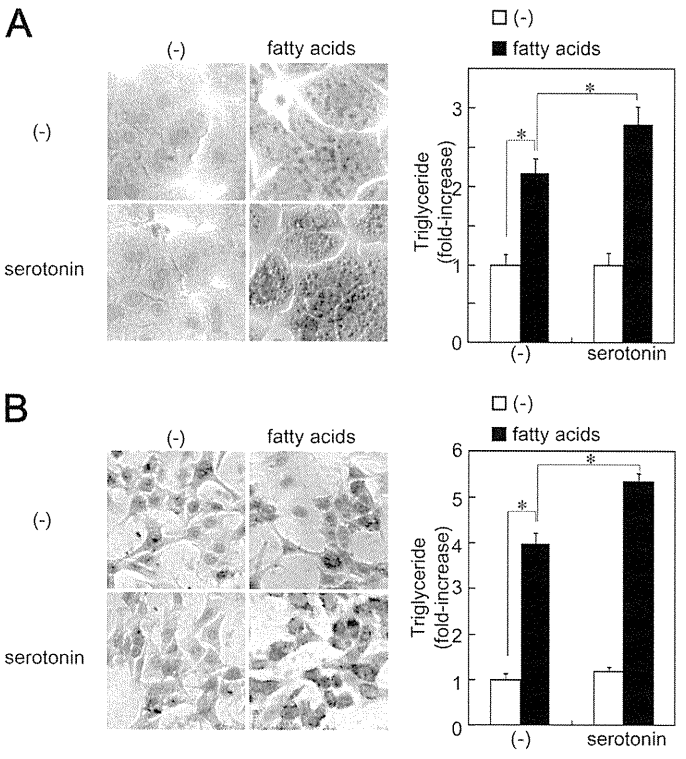

FIGURE 4. **Serotonin exacerbates lipid accumulation in hepatocytes.** Primary cultured mouse hepatocytes (*A*) or Hc hepatocytes (*B*) were treated with or without fatty acids (100 μM linoleic acid and 100 μM oleic acid) in the presence or absence of 100 μM serotonin for 18 h. Lipid droplets were assessed by Oil Red O staining (*left panels*; original magnification, ×400). Triglyceride levels in hepatocytes were determined (*right panel*). Results shown are representative of at least three independent experiments. Data are means ± S.D. from at least four independent experiments. *, $p < 0.05$.

Hepatic Autophagy Is Suppressed by L-Tryptophan/Serotonin Treatment—A high fat diet inhibits hepatic autophagy in mice (31), and the inhibition of autophagy in cultured hepatocytes and mouse livers showed an increase in triglyceride storage (25), suggesting that inhibited hepatic autophagy is involved in liver steatosis. Because mTOR is a master regulator of autophagy (21, 22) and an L-tryptophan/serotonin activated mTOR (Figs. 5 and 6), we examined the role of L-tryptophan/serotonin in hepatic autophagy by assessing LC3 aggregation and p62 degradation, which are hallmarks of autophagy. Although food deprivation induced LC3 aggregation and p62 degradation in the liver (supplemental Fig. 3*A*), HFHFD treatment suppressed the LC3 aggregation and p62 degradation (Fig. 7), indicating that autophagy is induced by cellular starvation but inhibited in steatotic hepatocytes. We found that L-tryptophan treatment suppressed LC3 aggregation and p62 degradation in mice with food deprivation (supplemental Fig. 3*A*), suggesting the inhibition of hepatic autophagy by L-tryptophan. Similarly, exogenous AADC expression, but not GFP or IDO expression, also suppressed LC3 aggregation and p62 degradation after food deprivation (supplemental Fig. 3*B*), suggesting that serotonin synthesis by introduction of AADC inhibits fasting-induced autophagy. As described above (supplemental Fig. 2), rapamycin improved hepatic steatosis. Similarly, rapa-

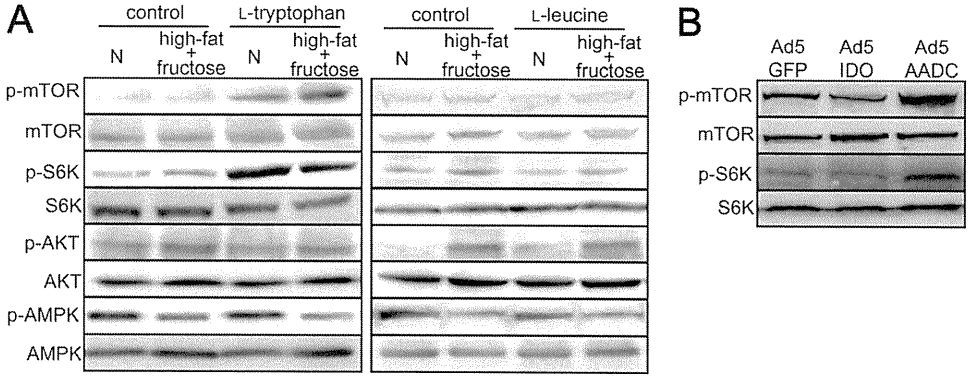

FIGURE 5. **L-Tryptophan induces mTOR activation.** *A*, mice were fed with normal diet (*N*) or HFHFD supplemented with or without L-tryptophan or L-leucine for 8 weeks. *B*, mice were infected with Ad5GFP, Ad5IDO, or Ad5AADC (5×10^8 pfu/mouse) and were humanely killed on 7 days after the adenoviral infection. Protein extracts from liver tissue or hepatocytes were subjected to immunoblot for phospho-mTOR, mTOR, phospho-p70S6K, p70S6K, phospho-AKT, AKT, phospho-AMPK, or AMPK, respectively. Results shown are representative of at least three independent experiments. The results of densitometric analysis are shown in supplemental Fig. 1*A*.

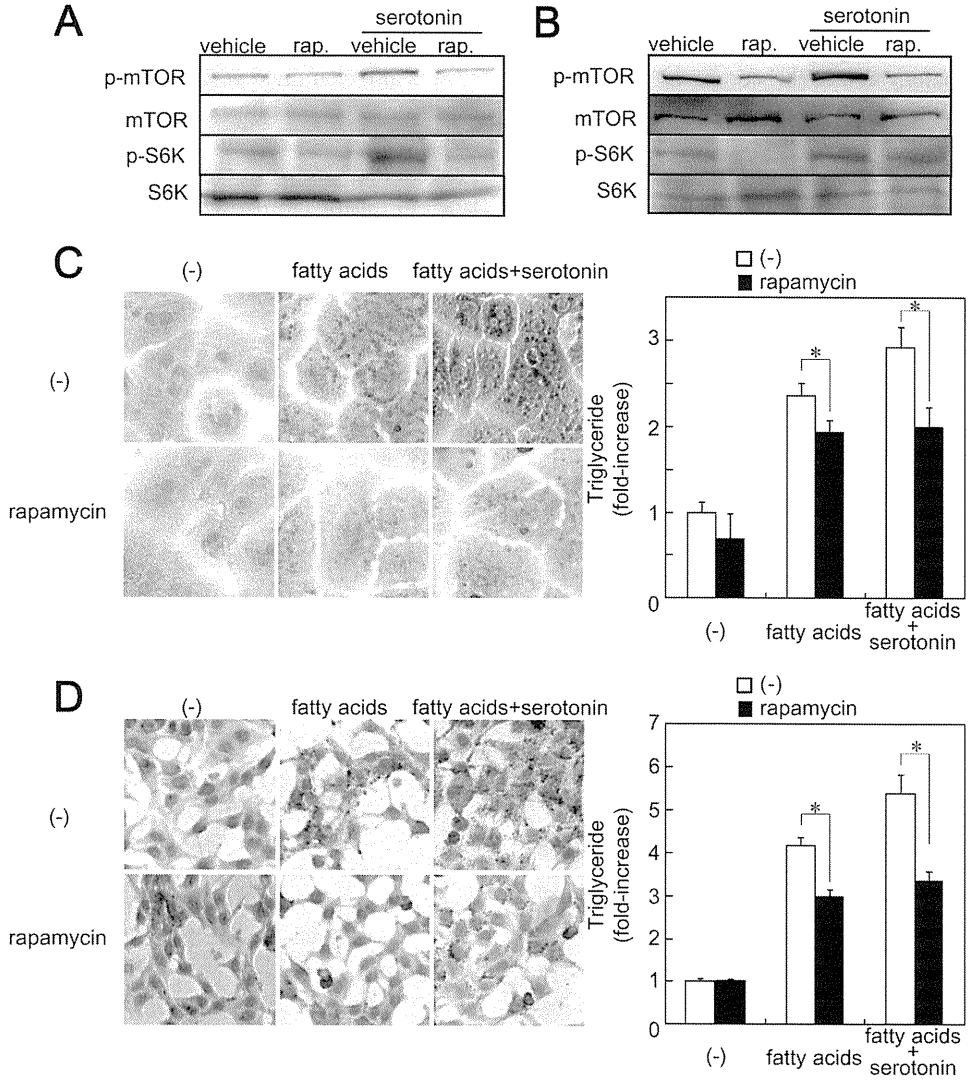

FIGURE 6. **Rapamycin improves lipid accumulation in hepatocytes.** Primary cultured mouse hepatocytes (*A* and *C*) or Hc hepatocytes (*B* and *D*) were pretreated with or without 100 nM rapamycin for 30 min. *A* and *B*, the hepatocytes were treated with or without 100 μM serotonin for 2 h. Protein extracts from hepatocytes at 2 h after the serotonin treatment were subjected to immunoblot for phospho-mTOR, mTOR, phospho-p70S6K, and p70S6K, respectively. *C* and *D*, the hepatocytes were treated with or without fatty acids (100 μM linoleic acid and 100 μM oleic acid) in the presence or absence of 100 μM serotonin for 18 h. Lipid droplets were assessed by Oil Red O staining (*left panels*; original magnification, ×400). Triglyceride levels in hepatocytes were determined (*right panel*). Results shown are representative of at least three independent experiments. Data are means ± S.D. from at least four independent experiments. *, $p < 0.05$. The results of densitometric analysis are shown in supplemental Fig. 1*B*.

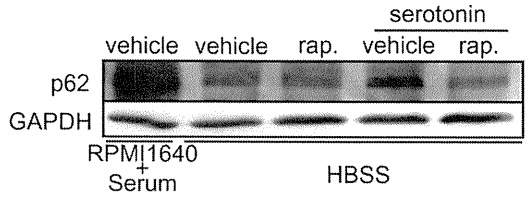

FIGURE 7. **Serotonin inhibits p62 degradation.** Hc hepatocytes were pretreated with or without rapamycin in HBSS. After 0.5 h of incubation, the cells were treated with or without serotonin and incubated for an additional 3 h. As a control, the cells were cultured in RPMI1640 medium containing FBS. Protein extracts were subjected to immunoblot for p62 or GAPDH, respectively. Results shown are representative of at least three independent experiments.

mycin treatment induced LC3 aggregation and p62 degradation in L-tryptophan-treated mice. These results demonstrated that inhibition of mTOR by rapamycin reversed L-tryptophan-mediated inhibition of autophagy (supplemental Fig. 3*C*), suggesting the ability of L-tryptophan to inhibit autophagy through mTOR. Subsequently, we examined whether serotonin suppresses autophagy through mTOR activation in hepatocytes. Hc hepatocytes were cultured in HBSS, amino acid-free conditions, for autophagy induction, and we assessed the levels of p62 (Fig. 7). In the Hc hepatocytes with starvation, autophagy was induced, as demonstrated by p62 degradation. Starvation-induced p62 degradation was inhibited by serotonin treatment, whereas rapamycin treatment induced p62 degradation in serotonin-treated cells. These results suggest that the inhibitory effects of L-tryptophan and serotonin on autophagy were reversed by inhibition of mTOR. This further suggests the suppression of hepatic autophagy as one of the possible mechanisms by which hepatic steatosis is enhanced by L-tryptophan/serotonin.

DISCUSSION

The present study examined the contribution of L-tryptophan to hepatic steatosis. L-Tryptophan has been reported to

induce hepatic steatosis in rats (5, 6). However, a conflicting report indicates that L-tryptophan does not cause fatty liver (32). In the present study, L-tryptophan treatment did not induce hepatic steatosis under normal diet conditions but had a stimulatory effect on hepatic steatosis when combined with HFHFD. HFHFD increased body weight, whereas the body/liver weight ratio was decreased. This indicates the accumulation of excess fat as body fat rather than visceral fat. In contrast, the combination of L-tryptophan and HFHFD exacerbated hepatic steatosis and reversed reduction of the body/liver weight ratio, which suggests that L-tryptophan induces accumulation of excess fat as visceral fat. This further suggests the overconsumption of L-tryptophan-rich protein (*e.g.* milk, cheese, meat, and sausage) as a possible cause of an aggravation of hepatic steatosis induced by excessive intake of fat and carbohydrate.

In addition to its role as a substrate for protein synthesis, L-tryptophan is the precursor of kynurenine and serotonin. Exogenous introduction of IDO by adenovirus or intraperitoneal administration of the IDO inhibitor 1-methyl-DL-tryptophan did not affect the lipid content of the liver (data not shown), suggesting a minor role of the kynurenine synthesis pathway in L-tryptophan-mediated biology on hepatic steatosis.

Adenoviral AADC introduction increased serum serotonin levels without decreasing L-tryptophan levels. In the serotonin synthesis pathway, a part of L-tryptophan is converted to 5-hydroxy-L-tryptophan by tryptophan hydroxylase and further converted to serotonin by AADC. L-Tryptophan is mostly used as material for protein synthesis, and a part of L-tryptophan may be used for serotonin synthesis. Thus, AADC increased serotonin levels without any changes in serum levels of tryptophan. Both L-tryptophan treatment and exogenous introduction of AADC increased lipid accumulation in the livers of mice fed with HFHFD. Moreover, an *in vitro* experiment using hepatocytes demonstrated that fatty acid-induced accumulation of lipid droplets and triglyceride synthesis were further increased by the treatment of serotonin. These findings suggest that serotonin is an essential component in the exacerbation of hepatic steatosis in L-tryptophan-treated mice.

Liver injury and fibrosis were induced in mice treated with HFHFD and L-tryptophan. Treatment with rapamycin attenuated liver injury and fibrosis with reduced hepatic steatosis. ROS formation plays a central role in the pathogenesis of liver damage and fibrosis in NASH (33). We found that L-tryptophan treatment significantly increased ROS production in the steatotic livers, which may be one of the central mechanisms by which L-tryptophan aggravates liver damage and fibrosis. A previous report demonstrated that serotonin-deficient tryptophan hydroxylase knock-out mice have reduced ROS, inflammation, and hepatocellular injury in NASH induced by a choline-methionine-deficient diet (9). This report is consistent with the other reports demonstrating that serotonin induces oxidative stress and mitochondrial toxicity in NASH (9). In addition, tryptophan itself can also induce oxidative stress (34). In the present study, L-tryptophan induced ROS formation in the steatotic livers, suggesting that L-tryptophan-mediated ROS formation requires lipid accumulation. In rat cerebral cortex tissue, L-tryptophan treatment reduces total radical-trapping antioxidant potential, total antioxidant reactivity, and glutathione levels (35). This suggests that suppression of antioxidants by L-tryptophan may one of the mechanisms of increased ROS formation in steatotic livers.

L-Tryptophan treatment increased hepatic mTOR phosphorylation after food deprivation (Fig. 5). Inhibition of mTOR by rapamycin reversed hepatic steatosis enhanced by L-tryptophan, suggesting that mTOR activation is a key for L-tryptophan-mediated exacerbation of hepatic steatosis. AKT is an upstream kinase in mTOR signaling (36) and is a key molecule for glucose and lipid metabolism. Sustained AKT activation in PTEN (phosphatase and tensin homolog on chromosome 10)-deleted livers induces fatty liver (37). In our model, food intake increased AKT and mTOR phosphorylation in mouse livers (data not shown). The HFHFD induced AKT phosphorylation but not mTOR phosphorylation under food-deprived conditions. In contrast, L-tryptophan treatment did not affect AKT phosphorylation, suggesting that L-tryptophan-mediated mTOR activation is not induced by AKT activation.

It has been reported that leucine regulates mTOR signaling, and acute administration of leucine induces phosphorylation of S6K in the liver (38) and the adipose tissue (39). Thus, we had to examine the specificity of the effect by L-tryptophan. We used L-leucine as a control amino acid. In contrast to L-tryptophan, phosphorylation of mTOR and S6K was not observed after L-leucine treatment. Our data are consistent with another previous report showing that chronic administration of leucine does not change S6K phosphorylation in the livers of rats (40) and neonatal pigs (41). Thus, L-tryptophan, but not L-leucine, induces activation of mTOR signaling.

Autophagy is activated by nutrient deprivation but inhibited by amino acids and/or released insulin after food intake (23). LC3 aggregation and p62 degradation, markers for autophagy, were induced in the liver after fasting. In contrast, the levels of LC3 aggregation and p62 degradation were suppressed in mice fed with HFHFD. This may be explained by hyperinsulinemia in mice fed a high fat diet (31). We also found L-tryptophan to have an inhibitory effect on hepatic autophagy (supplemental Fig. 3). Because L-tryptophan did not increase serum insulin level (data not shown), the effect of L-tryptophan may not be due to hyperinsulinemia. Instead, serotonin production was found to be crucial for L-tryptophan-mediated mTOR activation in the liver (Fig. 5). In combination with the previous report that serotonin treatment suppresses autophagy in hepatocellular carcinoma cells (42), our data suggest that L-tryptophan suppresses hepatic autophagy through serotonin production and mTOR activation. Because mTOR strongly inhibits autophagy and autophagy is important for regulating the breakdown of stored lipids (25), hepatic autophagy inhibited by L-tryptophan may be one of the mechanisms in the aggravation of hepatic steatosis.

In conclusion, L-tryptophan exacerbates hepatic steatosis by producing serotonin that activates mTOR signaling in mice fed with HFHFD. In addition to a calorie-restricted diet, targeting L-tryptophan may become a new therapeutic strategy for non-alcoholic fatty liver disease patients.

REFERENCES

1. Angulo, P. (2002) *N. Engl. J. Med.* **346,** 1221–1231
2. Sainio, E. L., Pulkki, K., and Young, S. N. (1996) *Amino Acids* **10,** 21–47
3. Zelber-Sagi, S., Nitzan-Kaluski, D., Goldsmith, R., Webb, M., Blendis, L., Halpern, Z., and Oren, R. (2007) *J. Hepatol.* **47,** 711–717
4. Richard, D. M., Dawes, M. A., Mathias, C. W., Acheson, A., Hill-Kapturczak, N., and Dougherty, D. M. (2009) *Int. J. Tryptophan. Res.* **2,** 45–60
5. Hirata, Y., Kawachi, T., and Sugimura, T. (1967) *Biochim. Biophys. Acta* **144,** 233–241
6. Trulson, M. E., and Sampson, H. W. (1986) *J. Nutr.* **116,** 1109–1115
7. Fears, R., and Murrell, E. A. (1980) *Br. J. Nutr.* **43,** 349–356
8. Toye, A. A., Dumas, M. E., Blancher, C., Rothwell, A. R., Fearnside, J. F., Wilder, S. P., Bihoreau, M. T., Cloarec, O., Azzouzi, I., Young, S., Barton, R. H., Holmes, E., McCarthy, M. I., Tatoud, R., Nicholson, J. K., Scott, J., and Gauguier, D. (2007) *Diabetologia* **50,** 1867–1879
9. Nocito, A., Dahm, F., Jochum, W., Jang, J. H., Georgiev, P., Bader, M., Renner, E. L., and Clavien, P. A. (2007) *Gastroenterology* **133,** 608–618
10. Lang, P. A., Contaldo, C., Georgiev, P., El-Badry, A. M., Recher, M., Kurrer, M., Cervantes-Barragan, L., Ludewig, B., Calzascia, T., Bolinger, B., Merkler, D., Odermatt, B., Bader, M., Graf, R., Clavien, P. A., Hegazy, A. N., Löhning, M., Harris, N. L., Ohashi, P. S., Hengartner, H., Zinkernagel, R. M., and Lang, K. S. (2008) *Nat. Med.* **14,** 756–761
11. Lesurtel, M., Soll, C., Graf, R., and Clavien, P. A. (2008) *Cell Mol. Life Sci.* **65,** 940–952
12. Yu, P. L., Fujimura, M., Okumiya, K., Kinoshita, M., Hasegawa, H., and Fujimiya, M. (1999) *J. Comp. Neurol.* **411,** 654–665
13. Facer, P., Polak, J. M., Jaffe, B. M., and Pearse, A. G. (1979) *Histochem. J.* **11,** 117–121
14. Kubovcakova, L., Krizanova, O., and Kvetnansky, R. (2004) *Neuroscience* **126,** 375–380
15. Guo, F., and Cavener, D. R. (2007) *Cell Metab.* **5,** 103–114
16. Macotela, Y., Emanuelli, B., Bång, A. M., Espinoza, D. O., Boucher, J., Beebe, K., Gall, W., and Kahn, C. R. (2011) *PLoS One* **6,** e21187
17. Laplante, M., and Sabatini, D. M. (2009) *Curr. Biol.* **19,** R1046–1052
18. Khamzina, L., Veilleux, A., Bergeron, S., and Marette, A. (2005) *Endocrinology* **146,** 1473–1481
19. Li, S., Brown, M. S., and Goldstein, J. L. (2010) *Proc. Natl. Acad. Sci. U.S.A.* **107,** 3441–3446
20. Chang, G. R., Chiu, Y. S., Wu, Y. Y., Chen, W. Y., Liao, J. W., Chao, T. H., and Mao, F. C. (2009) *J. Pharmacol. Sci.* **109,** 496–503
21. Dennis, P. B., Fumagalli, S., and Thomas, G. (1999) *Curr. Opin. Genet. Dev.* **9,** 49–54
22. Raught, B., Gingras, A. C., and Sonenberg, N. (2001) *Proc. Natl. Acad. Sci. U.S.A.* **98,** 7037–7044
23. Finn, P. F., and Dice, J. F. (2006) *Nutrition* **22,** 830–844
24. Czaja, M. J. (2010) *Am. J. Physiol. Cell Physiol.* **298,** C973–C978
25. Singh, R., Kaushik, S., Wang, Y., Xiang, Y., Novak, I., Komatsu, M., Tanaka, K., Cuervo, A. M., and Czaja, M. J. (2009) *Nature* **458,** 1131–1135
26. Osawa, Y., Uchinami, H., Bielawski, J., Schwabe, R. F., Hannun, Y. A., and Brenner, D. A. (2005) *J. Biol. Chem.* **280,** 27879–27887
27. Osawa, Y., Seki, E., Adachi, M., Suetsugu, A., Ito, H., Moriwaki, H., Seishima, M., and Nagaki, M. (2010) *Hepatology* **51,** 237–245
28. Osawa, Y., Seki, E., Kodama, Y., Suetsugu, A., Miura, K., Adachi, M., Ito, H., Shiratori, Y., Banno, Y., Olefsky, J. M., Nagaki, M., Moriwaki, H., Brenner, D. A., and Seishima, M. (2011) *FASEB J.* **25,** 1133–1144
29. Osawa, Y., Hannun, Y. A., Proia, R. L., and Brenner, D. A. (2005) *Hepatology* **42,** 1320–1328
30. Hoshi, M., Saito, K., Hara, A., Taguchi, A., Ohtaki, H., Tanaka, R., Fujigaki, H., Osawa, Y., Takemura, M., Matsunami, H., Ito, H., and Seishima, M. (2010) *J. Immunol.* **185,** 3305–3312
31. Liu, H. Y., Han, J., Cao, S. Y., Hong, T., Zhuo, D., Shi, J., Liu, Z., and Cao, W. (2009) *J. Biol. Chem.* **284,** 31484–31492
32. Matthies, D. L., and Jacobs, F. A. (1993) *J. Nutr.* **123,** 852–859
33. Lim, J. S., Mietus-Snyder, M., Valente, A., Schwarz, J. M., and Lustig, R. H. (2010) *Nat. Rev. Gastroenterol. Hepatol.* **7,** 251–264
34. Forrest, C. M., Mackay, G. M., Stoy, N., Egerton, M., Christofides, J., Stone, T. W., and Darlington, L. G. (2004) *Free Radic. Res.* **38,** 1167–1171
35. Feksa, L. R., Latini, A., Rech, V. C., Wajner, M., Dutra-Filho, C. S., de Souza Wyse, A. T., and Wannmacher, C. M. (2006) *Neurochem. Int.* **49,** 87–93
36. Drakos, E., Rassidakis, G. Z., and Medeiros, L. J. (2008) *Expert Rev. Mol. Med.* **10,** e4
37. Stiles, B., Wang, Y., Stahl, A., Bassilian, S., Lee, W. P., Kim, Y. J., Sherwin, R., Devaskar, S., Lesche, R., Magnuson, M. A., and Wu, H. (2004) *Proc. Natl. Acad. Sci. U.S.A.* **101,** 2082–2087
38. Reiter, A. K., Anthony, T. G., Anthony, J. C., Jefferson, L. S., and Kimball, S. R. (2004) *Int. J. Biochem. Cell Biol.* **36,** 2169–2179
39. Lynch, C. J., Halle, B., Fujii, H., Vary, T. C., Wallin, R., Damuni, Z., and Hutson, S. M. (2003) *Am. J. Physiol. Endocrinol. Metab.* **285,** E854–E863
40. Lynch, C. J., Hutson, S. M., Patson, B. J., Vaval, A., and Vary, T. C. (2002) *Am. J. Physiol. Endocrinol. Metab.* **283,** E824–E835
41. Wilson, F. A., Suryawan, A., Orellana, R. A., Gazzaneo, M. C., Nguyen, H. V., and Davis, T. A. (2011) *Amino Acids* **40,** 157–165
42. Soll, C., Jang, J. H., Riener, M. O., Moritz, W., Wild, P. J., Graf, R., and Clavien, P. A. (2010) *Hepatology* **51,** 1244–1254

The FASEB Journal • Research Communication

Acid sphingomyelinase regulates glucose and lipid metabolism in hepatocytes through AKT activation and AMP-activated protein kinase suppression

Yosuke Osawa,*,†,[1] Ekihiro Seki,§ Yuzo Kodama,§ Atsushi Suetsugu,† Kouichi Miura,§ Masayuki Adachi,§ Hiroyasu Ito,* Yoshimune Shiratori,† Yoshiko Banno,‡ Jerrold M. Olefsky,§ Masahito Nagaki,† Hisataka Moriwaki,† David A. Brenner,§ and Mitsuru Seishima*

*Department of Informative Clinical Medicine, †Department of Gastroenterology, and ‡Department of Cell Signaling, Gifu University Graduate School of Medicine, Gifu, Japan; and §Department of Medicine, University of California–San Diego School of Medicine, La Jolla, California USA

ABSTRACT **Acid sphingomyelinase (ASM) regulates the homeostasis of sphingolipids, including ceramides and sphingosine-1-phosphate (S1P). Because sphingolipids regulate AKT activation, we investigated the role of ASM in hepatic glucose and lipid metabolism. Initially, we overexpressed ASM in the livers of wild-type and diabetic *db/db* mice by adenovirus vector (Ad5ASM). In these mice, glucose tolerance was improved, and glycogen and lipid accumulation in the liver were increased. Using primary cultured hepatocytes, we confirmed that ASM increased glucose uptake, glycogen deposition, and lipid accumulation through activation of AKT and glycogen synthase kinase-3β. In addition, ASM induced up-regulation of glucose transporter 2 accompanied by suppression of AMP-activated protein kinase (AMPK) phosphorylation. Loss of sphingosine kinase-1 (SphK1) diminished ASM-mediated AKT phosphorylation, but exogenous S1P induced AKT activation in hepatocytes. In contrast, SphK1 deficiency did not affect AMPK activation. These results suggest that the SphK/S1P pathway is required for ASM-mediated AKT activation but not for AMPK inactivation. Finally, we found that treatment with high-dose glucose increased glycogen deposition and lipid accumulation in wild-type hepatocytes but not in $ASM^{-/-}$ cells. This result is consistent with glucose intolerance in $ASM^{-/-}$ mice. In conclusion, ASM modulates AKT activation and AMPK inactivation, thus regulating glucose and lipid metabolism in the liver.—Osawa, Y., Seki, E., Kodama, Y., Suetsugu, A., Miura, K., Adachi, M., Ito, H., Shiratori, Y., Banno, Y., Olefsky, J. M., Nagaki, M., Moriwaki, H., Brenner, D. A., Seishima, M. Acid sphingomyelinase regulates glucose and lipid metabolism in hepatocytes through AKT activation and AMP-activated protein kinase suppression. *FASEB J.* 25, 1133–1144 (2011). www.fasebj.org**

Key Words: sphingosine-1-phosphate · glucose intolerance · glucose transporter 2 · glycogen synthase kinase-3β

THE LIVER IS A KEY ORGAN for glucose and lipid metabolism. During feeding, hepatocytes increase glucose uptake in response to elevated glucose levels in the portal vein and increase glycogen and triacylglyceride synthesis. AKT is a key molecule for insulin signaling and glucose metabolism. On AKT activation, glucose influx is stimulated by activation of glycogen synthesis through glycogen synthase kinase (GSK)-3β. The facilitative glucose transporter (GLUT) 2 is predominantly expressed in the liver (1). Hepatic GLUT2 is located at the plasma membrane even in the absence of insulin stimulation; glucose uptake by GLUT2 is therefore not directly affected by insulin. Glucose increases GLUT2 mRNA levels in hepatocytes (2), resulting in increased glucose influx. Constitutive activity of AMP-activated protein kinase (AMPK) decreases glycogen synthesis accompanied by down-regulation of GLUT2 expression (3). Therefore, both AKT and AMPK are involved in glucose metabolism.

Acid sphingomyelinase (ASM) deficiency leads to Niemann-Pick disease. ASM has been reported to be involved in various cellular functions (4), including glucose and lipid metabolism. ASM activity is increased in the serum of type 2 diabetic patients (5). Sphingomyelinase induces GLUT4 translocation to the plasma membrane (6, 7) and increases glucose uptake by adipocytes (7, 8). A high-fat, high-cholesterol diet does not induce hepatic triacylglyceride accumulation in ASM-deficient mice ($ASM^{-/-}$) under an LDL receptor-deficient condition (9). ASM hydrolyzes sphingomyelin to ceramide and phosphorylcholine. Ceramide has been identified as a bioactive mediator in various

[1] Correspondence: Department of Informative Clinical Medicine, Gifu University Graduate School of Medicine, 1-1 Yanagido, Gifu, 501-1194, Japan. E-mail: osawa-gif@umin.ac.jp

doi: 10.1096/fj.10-168351

This article includes supplemental data. Please visit *http://www.fasebj.org* to obtain this information.

cellular functions, including apoptosis and the cell cycle (10, 11). Ceramide accumulation contributes to the development of type 2 diabetes (12). Indeed, inhibition of ceramide synthesis by myriocin, serine palmitoyltransferase inhibitor, or dihydroceramide desaturase improves insulin resistance induced by glucocorticoid or saturated fat (13). Ceramide induces insulin resistance by inactivation of AKT through protein phosphatase-2A and PKC-ζ (14, 15) or by inhibition of AKT translocation to the plasma membrane (16). In addition, ceramide inhibits AMPK activation in hepatoma cells (17).

Not only ceramide but also its metabolite sphingosine-1-phosphate (S1P) is involved in glucose metabolism. Ceramide is hydrolyzed by ceramidase to sphingosine, which is further phosphorylated to S1P by sphingosine kinase (SphK; ref. 18). S1P stimulates AKT activation in human (19) and rodent hepatocytes (20) through the S1P receptor (S1PR). S1P signaling also increases glucose uptake *via* the insulin receptor and production of reactive oxygen species in C2C12 mouse myoblast cells (21). Because sphingolipids are important in glucose and lipid metabolism, we investigated the role of ASM in glucose and lipid metabolism in hepatocytes. In this study, we determined that ASM stimulates glucose uptake, glycogen deposition, and lipid accumulation *via* S1P formation and subsequent AKT activation. As a result, ASM deficiency causes glucose intolerance.

MATERIALS AND METHODS

Animals

The experiments were conducted in accordance with the institutional guidelines of Gifu University and Columbia University. Sprague-Dawley male rats and male wild-type (C57BL/6J), $ASM^{-/-}$, SphK1-deficient ($SphK1^{-/-}$; refs. 20, 22), and obese and diabetic *db/db* mice (C57BL/6 background) were used for this study.

Mice

$ASM^{-/-}$ mice (C57BL/6 background) and $SphK1^{-/-}$ mice (C57BL/6 background) (23), which lack the putative lipid kinase catalytic domain, were bred for studies. Obese and diabetic *db/db* mice (C57BL/6 background) were obtained from the Institute for Animal Reproduction (Ibaragi, Japan), and wild-type C57BL/6J mice were from Japan SLC (Shizuoka, Japan). Eight- to 10-wk-old male mice were used for *in vivo* studies.

Intraperitoneal glucose tolerance test (IPGTT)

The 8- to 10-wk-old male mice (wild-type, *db/db*, or $ASM^{-/-}$ mice) were deprived of food for 18 h. D-Glucose (2 mg/g body weight) was injected intraperitoneally, and blood glucose levels were monitored at 0, 30, 60, and 120 min after the injection using G checker (Sanko Junyaku, Tokyo, Japan). Values for area under the blood glucose curve after glucose loading were calculated. Serum insulin content was measured with a mouse insulin ELISA kit (Shibayagi, Gunma, Japan).

Primary hepatocyte cultures

Sprague-Dawley male rats (200–250 g) or mice (4 wk old) were anesthetized with ketamine and xylazine administered by intraperitoneal injection. Hepatocytes were then isolated by a nonrecirculating *in situ* collagenase perfusion of livers cannulating through the portal vein of rats or inferior vena cava of mice. Livers were first perfused *in situ* with 0.5 mM EGTA containing calcium-free salt solution, followed by perfusion with solution containing 0.02% collagenase D (Roche Diagnostics, Indianapolis, IN, USA). The liver was then gently minced on a Petri dish and filtered with polyamide mesh (3-60/42; Sefar America Inc., New York, NY, USA). Hepatocytes were washed 3 times and centrifuged at 50 *g* for 1 min. Cell viability was consistently >90%, as determined by trypan blue exclusion. Cells were plated on dishes coated with rat collagen type I in Waymouth medium (Invitrogen, Carlsbad, CA, USA) containing 10% fetal bovine serum with antibiotics (plating medium).

Cell treatment

After isolation from rat or mouse livers, hepatocytes were cultured in 10% FBS-containing medium for 4 h. Cells were then washed twice with PBS and changed to serum-free RPMI 1640 (Invitrogen) containing glucose (200 mg/dl) and antibiotics in the presence or absence of recombinant adenoviruses [10 plaque forming units (PFU)/cell]. After a 2-h incubation, the culture medium was changed to serum-free RPMI 1640 containing antibiotics, and the cells were incubated for an additional 16 h. Before stimulation with ASM (1 IU/ml; Sigma-Aldrich, St. Louis, MO, USA), SIP (1 μM; Sigma-Aldrich), or high-dose glucose (600 mg/dl), the cells were washed twice with PBS. The cells were pretreated with imipramine (50 μM; Sigma-Aldrich) for 1 h or with pertussis toxin (PTX) (Sigma-Aldrich) for 16 h in some experiments. The hepatocytes were then treated with or without ASM, SIP, or high-dose glucose, and incubated 8 h for glycogen, RNA, and protein extraction or 24 h for Oil Red O staining and triglyceride measurement. The experimental design is shown in Supplemental Fig. S1*A*.

Recombinant adenoviruses

The adenovirus 5 (Ad5) variants Ad5GFP, Ad5CA-AKT, Ad5DN-AKT, Ad5CA-AMPK, and Ad5DN-AMPK express green fluorescent protein (GFP), constitutively active (CA)-AKT encoding an amino-terminal myristylation signal, dominant-negative (DN)-AKT, c-*myc*-CA-AMPK, and c-*myc*-DN-AMPK, respectively (20, 24). The recombinant replication deficient adenovirus Ad5ASM expressing ASM was constructed by an AdEasy Adenoviral Vector System (Stratagene, La Jolla, CA, USA). In brief, the full length of human ASM DNA was subcloned into pTrack adenoviral vector. The plasmid DNA was prepared by the alkaline lysis method and transfected into BJ5183-AD-1 electroporation-competent cells. The virus was grown in HEK293 cells and purified by banding twice on CsCl gradients, then dialyzed and stored at −20°C. The pTrack plasmid contains a GFP sequence driven under a CMV promoter, and the Ad5ASM expresses both ASM and GFP. Mice were infected with the adenoviruses (5×10^8 PFU/mouse) by intravenous injection. IPGTT was performed on 3 d after the infection. The animals were humanely killed at 3 d for glycogen and protein extraction and at 7 d for Oil Red O staining and triglyceride measurement.

Glucose uptake

Primary cultured hepatocytes were treated with or without ASM for 2 h or infected with Ad5ASM or Ad5GFP, and then

2-deoxy-D-[1-^{3}H]glucose (2 μCi/ml; Amersham Biosciences, Piscataway, NJ, USA) was added to the culture medium. After a further 1-h incubation, cells were washed 3 times with ice-cold PBS and lysed in 1% SDS and 200 mM NaOH. The amount of labeled glucose taken up was determined by scintillation counting.

Measurement of glycogen content

After the treatment of hepatocytes for the indicated periods, the dish was placed on ice, washed with ice-cold PBS twice, and then incubated with 30% KOH for 30 min at room temperature. For the measurement of glycogen content in liver tissue, frozen liver tissues were homogenized in 30% KOH. Then, ethanol was added to the lysate, and glycogen was precipitated by centrifugation. The pellet was dissolved with H_2O, and glycogen content was determined by anthrone reagent (2 mg anthrone/ml sulfuric acid). Glucose solution was used as a standard.

Oil Red O staining

For lipid droplet staining, the cells were fixed with 10% formalin and stained with Oil Red O working solution. Hematoxylin was used for counterstaining. For liver tissue, the frozen liver sections were cut at a thickness of 5 μm on a cryostat and stained with Oil Red O.

Measurement of triglyceride

After the treatment, the primary cultured hepatocytes were washed with PBS and scraped with methanol. For the measurement of triglyceride in liver tissue, frozen liver tissues were homogenized in PBS, and methanol was added to the lysate. The lipids were extracted by the method of Bligh and Dyer (25), and triglyceride content was measured using a triglyceride kit (L-type TG M with lipid calibrator; Wako, Osaka, Japan).

Western blot

For the preparation of total cell proteins, cells or frozen liver tissues were homogenized in radioimmunoprecipitation assay buffer (50 mM Tris-HCl, pH 8.8; 150 mM NaCl; 10 mM EGTA; 1% Triton-X; 0.1% SDS; 1% deoxycholic acid; 0.3 mM PMSF; 1 mM sodium orthovanadate; 10 mM sodium fluoride; 0.1 mM sodium molybdate; and 0.5 mM 4-deoxypyridoxine). The proteins were separated by SDS-PAGE and were electrophoretically transferred onto nitrocellulose membrane. The membranes were first incubated with the primary antibodies, anti-phosphorylated-AKT (Ser-473; 9271; Cell Signaling Technology, Danvers. MA, USA), AKT (9272; Cell Signaling), phosphorylated-GSK3β (Ser-9, 9336; Cell Signaling), GSK3β (610201; BD Biosciences, San Jose, CA, USA), phosphorylated-AMPKα (Thr-172, 2531; Cell Signaling), AMPKα (2603; Cell Signaling), GLUT2 (sc-9116; Santa Cruz Biotechnology, Santa Cruz, CA, USA), ASM (sc-11352; Santa Cruz Biotechnology), and β-actin (Sigma-Aldrich) antibodies. Then, the membrane was incubated with the horseradish peroxidase-coupled secondary antibodies (Santa Cruz Biotechnology). Detection was performed with an ECL system (Amersham Biosciences), and the protein bands were quantified by densitometry using the ImageJ program (U.S. National Institutes of Health; http://rsb.info.nih.gov/ij/).

Quantitative real-time RT-PCR

Extracted RNA from the cells was reverse-transcribed, and quantitative real-time PCR with probe-primer sets of GLUT2 and 18S ribosomal RNA (Applied Biosystems, Foster City, CA, USA) was performed using TaqMan analysis (ABI Prism 7000; Applied Biosystems). The changes were normalized based on 18S.

Mass spectrometric analysis of sphingolipids

Electrospray ionization tandem mass spectrometry analysis was performed on a Thermo Finnegan TSQ 7000 triple quadruple mass spectrometer (Thermo Finnegan, San Jose, CA, USA), operating in multiple reaction monitoring positive ionization mode, as reported previously (26).

S1P formation

Primary rat hepatocytes were incubated with [^{3}H]serine (2 μCi/ml)-containing medium for 12 h. Then, the medium was changed to serum-free RPMI 1640 medium containing [^{3}H]serine with subsequent incubation with adenoviruses for an additional 18 h. The cellular lipids were extracted by the method of Bligh and Dyer (25) and separated on TLC plates in the solvent system of 1-butanol/acetic acid/water (60:20:20, v/v). The radiolabeled S1P spot was scraped off from the plates, and the radioactivity was measured in a liquid scintillation counter.

Statistical analysis

The results shown are representative of ≥3 independent experiments. Data are expressed as means ± SD from ≥4 independent experiments. Data between groups were analyzed by Student's *t* test. Values of $P < 0.05$ were considered statistically significant.

RESULTS

Exogenous ASM improves glucose metabolism in mice

To explore the role of hepatic ASM on glucose and lipid metabolism, an adenovirus vector expressing human ASM, Ad5ASM, was used in this study. On administration of Ad5ASM into mice, ASM was preferentially expressed in the liver but not in muscle and adipose tissue (Supplemental Fig. S1*B, C*). As a result, ASM activity in the liver was increased (Supplemental Fig. S1*D*). Sufficient expression and activity of ASM in Ad5ASM-infected primary cultured hepatocytes were confirmed. This activity efficiently suppressed the level of sphingomyelins in hepatocytes (Supplemental Fig. S1*E* and **Table 1**). Initially, we investigated the effect of ASM in a glucose tolerance test and demonstrated that blood glucose levels were decreased in both wild-type (**Fig. 1*A***) and diabetic *db/db* mice (Fig. 1*B*) in which ASM was overexpressed by Ad5ASM, indicating that ASM improves glucose tolerance. Then, we used primary cultured hepatocytes to investigate the effect of ASM on glucose uptake. Exogenous administration or adenoviral introduction of ASM increased glucose up-

TABLE 1. *Changes in the sphingolipid profile in Ad5ASM-infected hepatocytes*

Species	Ad5GFP	Ad5ASM
C14-SphM	31.5 ± 0.1	22.2 ± 1.8*
C16-SphM	6626.5 ± 261.3	4376.0 ± 210.8*
C18-SphM	2053.2 ± 65.0	1108.7 ± 53.4*
C18:1-SphM	260.9 ± 5.8	168.7 ± 5.1*
C20-SphM	1062.2 ± 20.0	564.4 ± 84.2*
C20:1-SphM	130.0 ± 2.6	79.3 ± 5.5*
C22-SphM	8397.5 ± 538.7	5223.5 ± 688.8*
C22:1-SphM	1221.8 ± 60.2	696.0 ± 109.1*
C24-SphM	24,630.7 ± 115.6	16,310.1 ± 2479.5*
C24:1-SphM	17,194.4 ± 630.6	10,981.6 ± 1385.0*
C14-Cer	5.8 ± 0.6	7.1 ± 1.5
C16-Cer	181.5 ± 7.5	185.3 ± 4.3
C18-Cer	39.3 ± 5.5	50.4 ± 1.3*
C-18:1-Cer	8.4 ± 0.9	10.1 ± 0.1*
C20-Cer	33.0 ± 5.1	42.8 ± 1.5
C24-Cer	919.8 ± 70.5	1140.7 ± 82.5*
C24:1-Cer	547.0 ± 70.3	598.4 ± 3.8
Sph	140.3 ± 19.0	248.6 ± 14.5*

Primary cultured rat hepatocytes were infected with Ad5GFP or Ad5ASM. Sphingomyelin and the different ceramide species were examined by mass spectrometric analysis. Results are expressed as picomoles lipid per milligram protein; they represent means ± SD from 3 independent experiments. SphM, sphingomyelin; Cer, ceramide; Sph, sphingosine. *$P < 0.05$.

take in hepatocytes (Fig. 1*C*), suggesting that ASM improves glucose tolerance by increased hepatic glucose uptake. Next, we examined the role of ASM in glycogen synthesis. Exogenous ASM expression increased hepatic glycogen content *in vivo* (Fig. 1*D*) and *in vitro* (Fig. 1*E*) using primary cultured hepatocytes. We further examined the role of ASM in lipid metabolism. Exogenous ASM introduction increased hepatic lipid content and serum triglycerides (**Fig. 2*A*, *B***) *in vivo*. We verified that ASM induces accumulation of lipid droplets and triglyceride in primary cultured hepatocytes (Fig. 2*C*). These results indicate that ASM contributes not only to glucose uptake but also to the synthesis of glycogen and triglyceride in the liver.

ASM induces AKT activation

AKT is a key molecule in insulin signaling and glucose metabolism. We hypothesized that AKT is involved in ASM-mediated glucose, glycogen, and lipid metabolism. To prove this, we initially investigated whether AKT affects glucose and lipid metabolism in hepatocytes using adenoviral overexpression of DN- or CA-AKT (Ad5DN-AKT and Ad5CA-AKT, respectively). DN-AKT inhibited insulin-induced phosphorylation of AKT, thereby inhibiting glycogen deposition and lipid accumulation by insulin or high-dose glucose in primary cultured hepatocytes (data not shown). In contrast, a constitutively active form of AKT strongly phosphorylated GSK3β (Supplemental Fig. S2*A*), resulting in increased glycogen deposition and lipid accumulation (Supplemental Fig. S2*B* and data not shown). AKT is therefore crucial for glucose and lipid

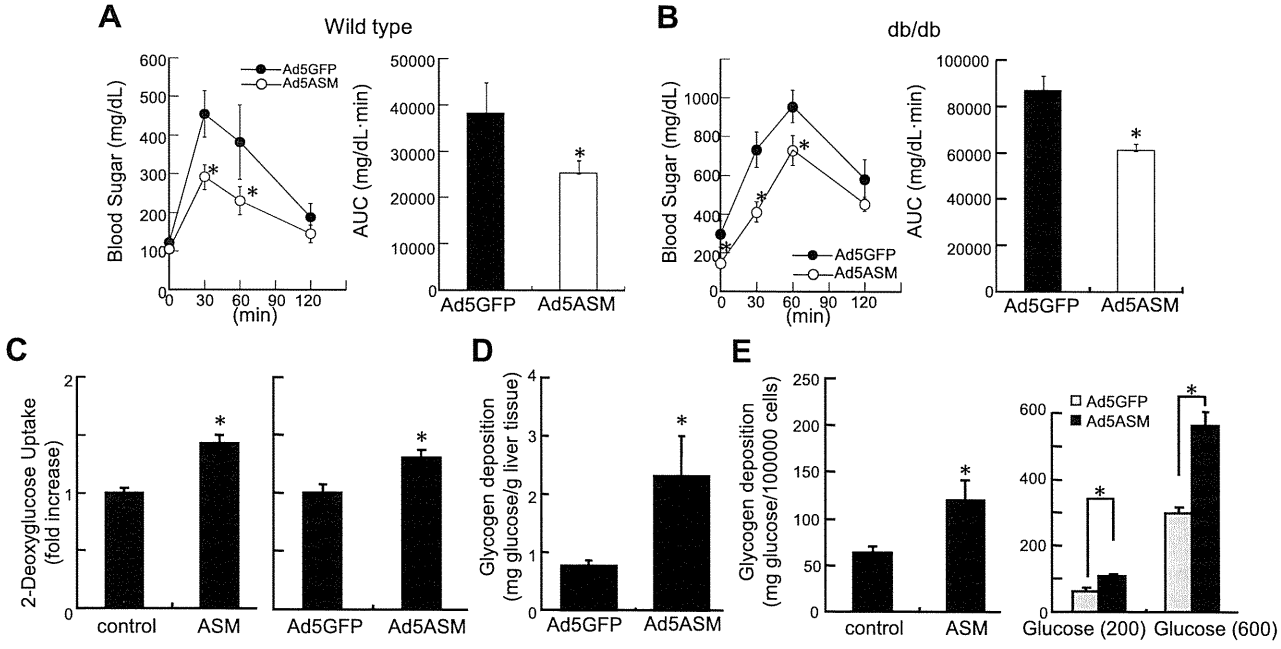

Figure 1. Ad5ASM improves glucose tolerance in mice. *A*, *B*) Wild-type (*A*) or diabetic *db/db* mice (*B*) were infected with Ad5GFP or Ad5ASM (5×10^8 PFU/mouse), then deprived of food for 18 h, and IPGTT was performed by administering a glucose load of 2 mg/g body weight 3 d after the infection. Values of area under the blood glucose curve were calculated (right panels). *C*) Primary cultured rat hepatocytes were treated with ASM (1 U/ml) for 2 h (left panel) or infected with Ad5GFP or Ad5ASM (10 PFU/cell; right panel), followed by measurement of 2-deoxy-D-[1-^{3}H]glucose uptake after a 1-h incubation period. *D*) Hepatic glycogen content in wild-type mice was determined under food-deprivation conditions at 3 d after the adenoviral infection. *E*) Glycogen content was determined in rat hepatocytes at 8 h after ASM treatment (left panel) or normal (200 mg/dl) and high-dose glucose (600 mg/dl) (right panel) treatment with Ad5GFP or Ad5ASM infection. Data are means ± SD from ≥4 independent experiments. *$P < 0.05$.

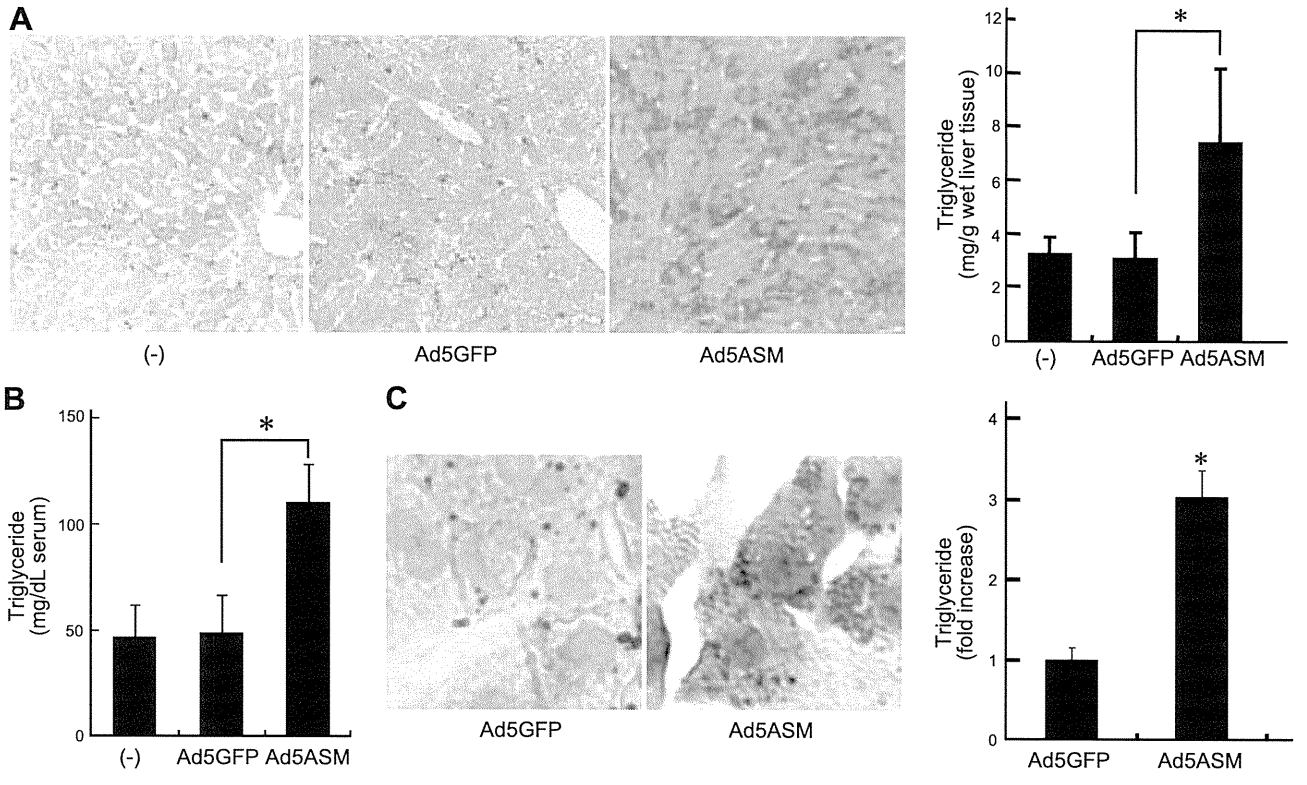

Figure 2. ASM stimulates lipid accumulation. *A*) Wild-type mice were infected with Ad5GFP or Ad5ASM (5×10^8 PFU/mouse). Hepatic lipid content was assessed by Oil Red O staining (left panel; original view ×200) and triglyceride measurement (right panel) in food-deprived wild-type mice at 7 d after the adenovirus infection. *B*) Serum triglycerides were determined in food-deprived wild-type mice at 7 d after the infection. *C*) Primary cultured rat hepatocytes were infected with Ad5GFP or Ad5ASM (10 PFU/cell). Lipid droplets were assessed by Oil Red O staining (original view ×800). Triglyceride level in hepatocytes was determined (right panel). Data are means ± SD from ≥4 independent experiments. $^*P < 0.05$.

metabolism in hepatocytes. On the basis of the fundamental roles of AKT in glucose and lipid metabolism, we investigated the role of AKT in ASM-mediated glucose, glycogen, and lipid metabolism. First, we examined whether ASM alters AKT signaling. Food intake stimulates AKT and GSK3β phosphorylation in mouse liver (**Fig. 3*A***). Introduction of exogenous ASM increased AKT activation under food-deprivation conditions and further increased under feeding conditions (Fig. 3*A*) without increasing serum insulin levels (data not shown) in comparison with control virus-infected animals. We further tested the requirement for insulin in ASM-induced AKT activation. In insulin-free conditions, introduction of ASM still increased AKT and GSK3β phosphorylation in primary cultured rat hepatocytes (Fig. 3*B*, left panel). High-dose glucose did not affect AKT and GSK3β phosphorylation in primary hepatocytes (Fig. 3*B*, left panel). These results suggest that ASM-induced AKT activation is not mediated by insulin or a response to increased intracellular glucose. In contrast, overexpression of DN-AKT abolished ASM-mediated AKT and GSK3β activity (Fig. 3*B*, right panel). DN-AKT overexpression also abolished ASM-induced glycogen deposition and lipid accumulation (Fig. 3*C, D*). These results suggest that ASM regulates glucose, glycogen, and lipid metabolism *via* activation of AKT.

ASM decreases AMPK phosphorylation and increases GLUT2 expression in hepatocytes

Because AMPK is an important component in glucose metabolism, the effects of ASM on AMPK signaling were examined. Glycogen deposition induced by high-dose glucose was increased by DN-AMPK and reduced by CA-AMPK (Supplemental Fig. S2*C, D*) with no observed effects on AKT and GSK3β phosphorylation (data not shown), indicating that AMPK activation reduced glycogen synthesis; this result is consistent with previous studies (3). Then, we assessed the role of AMPK in ASM-mediated effects. In the control virus-infected livers, food intake did not affect AMPK phosphorylation (**Fig. 4*A***), consistent with a previous report (27). In contrast, introduction of ASM reduced AMPK phosphorylation in response to food intake (Fig. 4*A*). ASM also increased food intake-related GLUT2 protein expression in the liver (Fig. 4*A*). A previous study gave indirect evidence that high glycogen content represses AMPK activation in skeletal muscle (28). However, our data demonstrated that AMPK phosphorylation was reduced by ASM in primary cultured hepatocytes under normal glucose conditions (Fig. 4*B*), in which the glycogen content was lower than that in Ad5GFP-infected cells cultured in high-dose glucose medium (Fig. 1*E*). These results suggest that the AMPK inactivation by ASM is not mediated by a response to increased intracellular glycogen. In primary cultured hepatocytes,

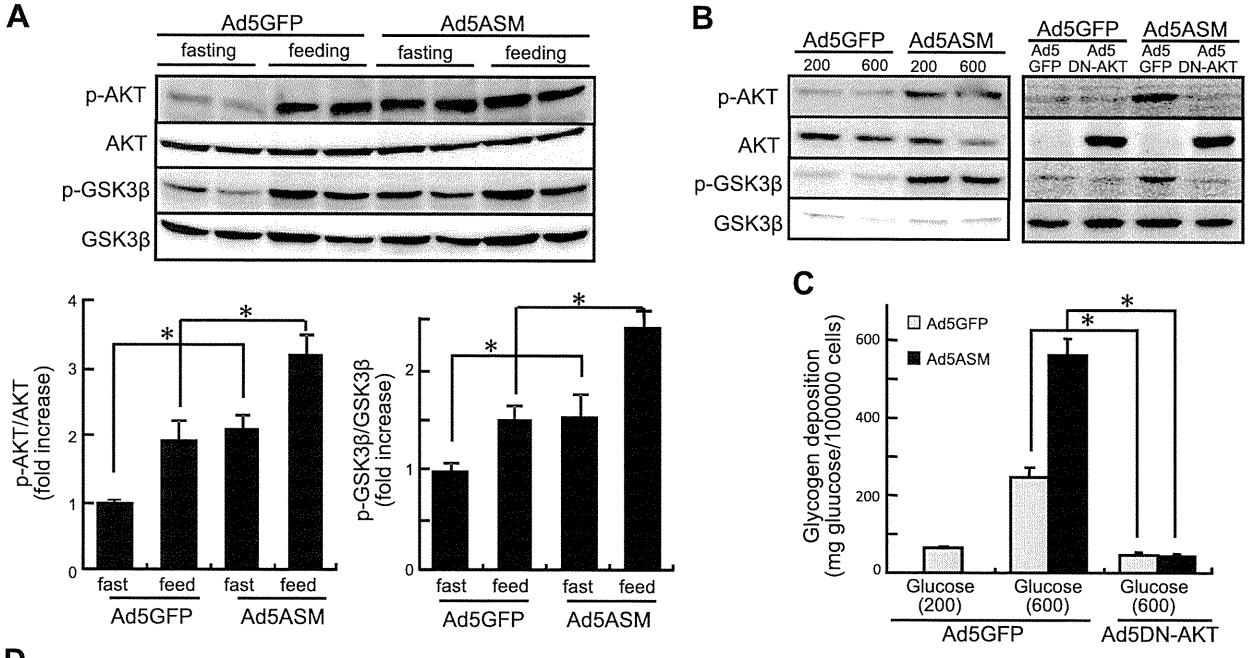

Figure 3. DN-AKT eliminates the effect of ASM introduction. *A*) Wild-type mice were infected with Ad5GFP or Ad5ASM (5×10^8 PFU/mouse), and the animals were killed in both nonfeeding (fasting; 18 h food deprivation) and feeding conditions at 3 d after the adenoviral infection. Protein extracts from liver tissue were subjected to immunoblot for phosphorylated (p)-AKT, AKT, p-GSK3β, and GSK3β. Relative densitometric intensity of p-AKT and p-GSK3β was determined for each protein band and normalized to AKT and GSK3β, respectively (bottom panels). *B*) Primary cultured rat hepatocytes infected with Ad5GFP or Ad5ASM (10 PFU/cell) were further infected with Ad5GFP or Ad5DN-AKT or treated with or without high-dose glucose (600 mg/dl; normal glucose, 200 mg/dl) for 8 h. Protein extracts from hepatocytes were subjected to immunoblot for p-AKT, AKT, p-GSK3β, and GSK3β. *C*) Primary cultured rat hepatocytes infected with Ad5GFP or Ad5ASM plus Ad5GFP or Ad5DN-AKT were treated with or without high-dose glucose. Glycogen content was determined in hepatocytes at 8 h after the high-dose glucose treatment. *D*) Primary cultured rat hepatocytes were infected with Ad5GFP or Ad5ASM plus Ad5GFP or Ad5DN-AKT. Lipid droplets were assessed by Oil Red O staining in hepatocytes (original view ×800). Results shown are representative of ≥3 independent experiments. Data are means ± SD from ≥4 independent experiments. $^*P < 0.05$.

high-dose glucose slightly reduced AMPK phosphorylation (Fig. 4*B*), as shown in a previous report in HepG2 hepatoblastoma cells (29), suggesting that the refractoriness of AMPK by food intake was probably due to systemic mediators. In addition to AMPK, GLUT2 protein and mRNA levels were increased in ASM-expressing primary hepatocytes (Fig. 4*B*, *C*). CA-AMPK partially inhibited glycogen deposition and lipid accumulation induced by ASM (Fig. 4*D*, *E*). These results suggest that reduced AMPK activation is also crucial for ASM-mediated glucose metabolism.

ASM activates AKT through the SphK/S1P pathway

ASM hydrolyzes sphingomyelin into ceramide, which is further hydrolyzed and phosphorylated by ceramidase and SphK to form S1P. Because S1P activates AKT in hepatocytes (20), we investigated the contribution of S1P generation to ASM-mediated glucose and lipid metabolism. The ASM-induced phosphorylation of AKT and GSK3β was reduced in SphK1$^{-/-}$ hepatocytes (**Fig. 5*A***). Of note, S1P formation was inhibited in SphK1$^{-/-}$ cells (Fig. 5*B*, left panels). Overexpression of neutral ceramidase (NCD) or exogenous S1P activated AKT (Fig. 5*B*, middle and right panels) in hepatocytes, as we reported previously (20). These results suggest that S1P generated by the breakdown of sphingomyelin contributes to ASM-induced AKT activation. We then examined the involvement of S1PR. Hepatocytes were treated with PTX because S1PRs coupled with G_i are sensitive to PTX. ASM-mediated AKT activation was reduced by PTX treatment (Fig. 5*C*), indicating that ASM generates S1P, which further activates AKT, at least partially *via* S1PRs. ASM-induced glycogen deposition and lipid accumulation were also reduced in SphK1$^{-/-}$ hepatocytes (**Fig. 6*A*, *B***), whereas the sphingomyelin and ceramide levels were similar to those in wild-type hepatocytes (data not shown). Moreover, SphK1$^{-/-}$ mice did not show hepatic steatosis by exogenous ASM introduction (Fig. 6*C*). In contrast to

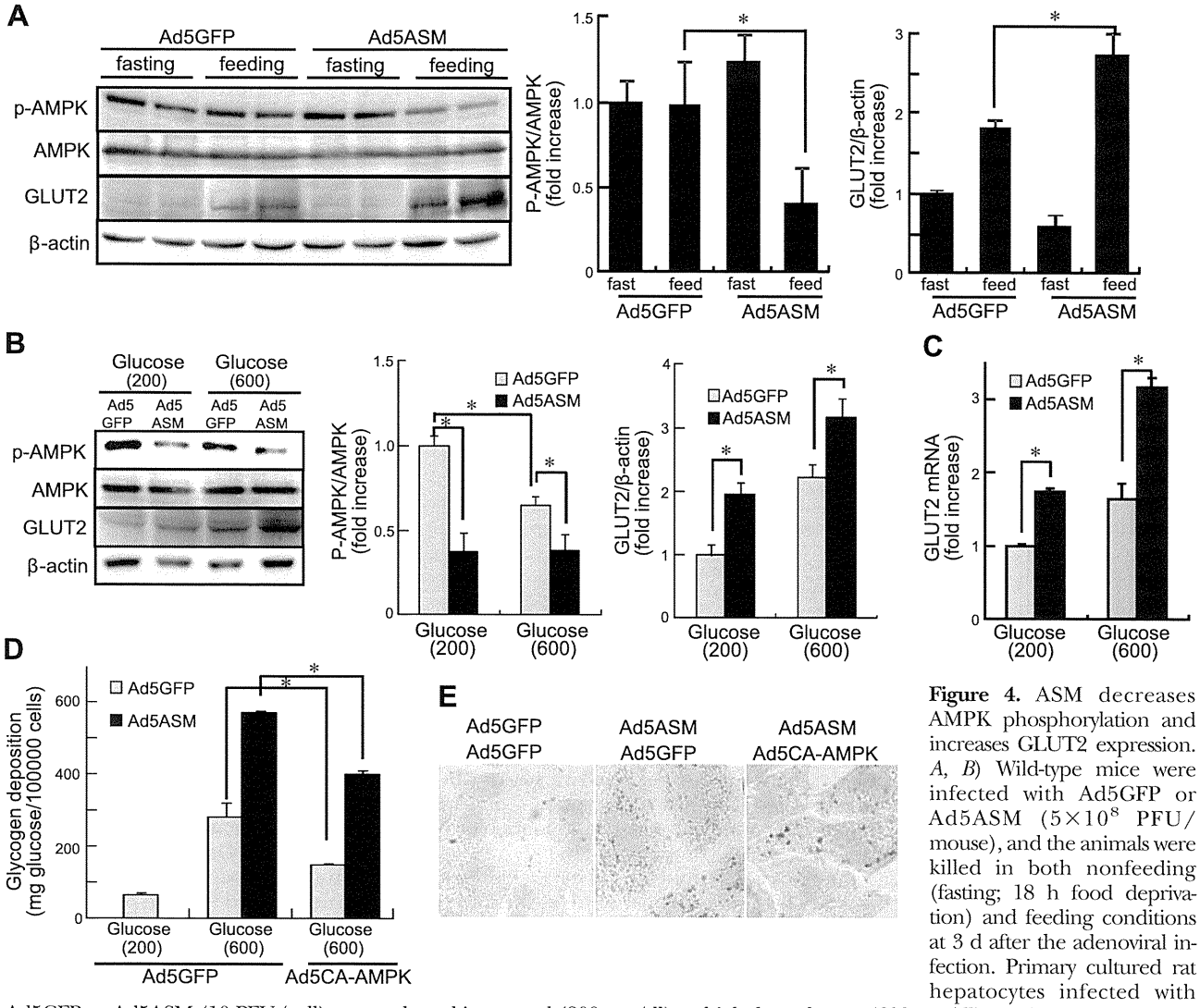

Figure 4. ASM decreases AMPK phosphorylation and increases GLUT2 expression. *A, B*) Wild-type mice were infected with Ad5GFP or Ad5ASM (5×10^8 PFU/mouse), and the animals were killed in both nonfeeding (fasting; 18 h food deprivation) and feeding conditions at 3 d after the adenoviral infection. Primary cultured rat hepatocytes infected with Ad5GFP or Ad5ASM (10 PFU/cell) were cultured in normal (200 mg/dl) or high-dose glucose (600 mg/dl) conditions for 8 h. Left panels: protein extracts from the liver tissue (*A*) or the hepatocytes (*B*) were subjected to immunoblot for phosphorylated (p)-AMPK, AMPK, GLUT2, and β-actin. Right panels: relative densitometric intensity of p-AMPK and GLUT2 was determined for each protein band and normalized to AMPK and β-actin, respectively. *C*). mRNA levels of GLUT2 in hepatocytes were determined by quantitative real-time RT-PCR and normalized by 18S ribosomal RNA. *D*) Primary cultured rat hepatocytes infected with Ad5GFP or Ad5CA-AMPK were further infected with Ad5GFP or Ad5ASM. Cells were then incubated in normal or high-dose glucose conditions for 8 h. Glycogen content in hepatocytes was determined. *E*) Primary cultured rat hepatocytes were infected with Ad5GFP, Ad5CA-AMPK, and/or Ad5ASM. Lipid droplets in hepatocytes were assessed by Oil Red O staining (original view ×800). Results shown are representative of ≥3 independent experiments. Data are means ± SD from ≥4 independent experiments. $^*P < 0.05$.

AKT, AMPK was not affected by S1P administration or NCD overexpression (Fig. 5*B*, middle panel). As in wild-type mice, SphK1$^{-/-}$ mice expressing exogenous ASM showed decreased phosphorylation of AMPK (Fig. 5*A*), indicating that the SphK/S1P pathway is not required for ASM-induced AMPK down-regulation.

ASM deficiency inhibits glucose uptake, glycogen deposition, and lipid accumulation in hepatocytes

Finally, we tested whether ASM deficiency causes glucose intolerance. Sphingomyelin accumulation and ceramide reduction were observed in hepatocytes isolated from ASM$^{-/-}$ mice (Supplemental Table S1). Blood glucose levels in ASM$^{-/-}$ mice were higher than those in ASM$^{+/+}$ mice throughout the IPGTT period without any changes in insulin levels (**Fig. 7**). To further investigate the specific role of ASM in hepatocytes, primary hepatocytes were isolated and treated with high-dose glucose (600 mg/dl), which increased glycogen levels (**Fig. 8*A***). Imipramine, a tricyclic antidepressant, causes proteolysis of the active 72-kDa ASM form, thus inhibiting ASM activity (30). Pretreatment with imipramine inhibited high-dose glucose-induced glycogen deposition (Fig. 8*A*), as did the knockout of ASM in mouse hepatocytes (Fig. 8*B*). Moreover, high-dose glucose increased lipid droplets in primary hepatocytes, and imipramine or ASM deficiency suppressed this effect (Fig. 8*C, D*). These results suggest that high-dose glucose increases glucose uptake, resulting in glycogen deposition and lipid accumulation in hepato-

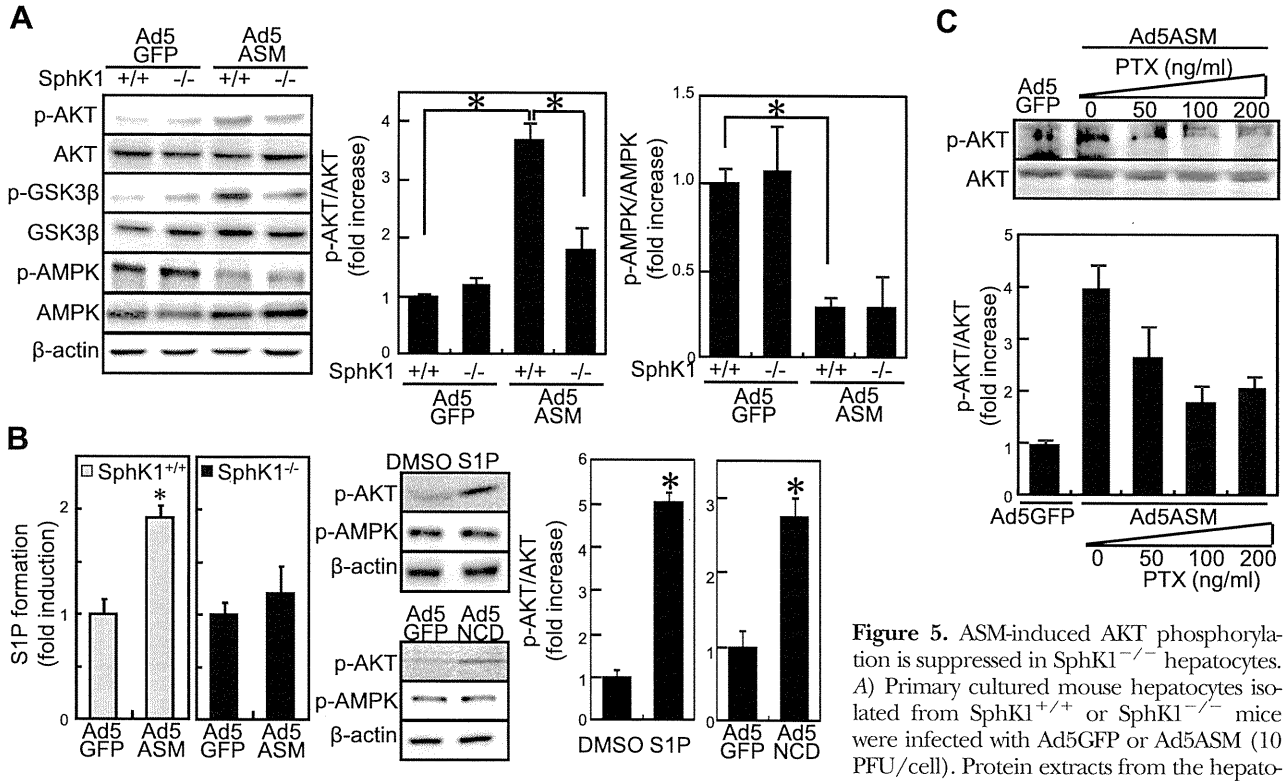

Figure 5. ASM-induced AKT phosphorylation is suppressed in SphK1$^{-/-}$ hepatocytes. *A*) Primary cultured mouse hepatocytes isolated from SphK1$^{+/+}$ or SphK1$^{-/-}$ mice were infected with Ad5GFP or Ad5ASM (10 PFU/cell). Protein extracts from the hepatocytes were subjected to immunoblot for phosphorylated (p)-AKT, AKT, p-GSK3β, GSK3β, p-AMPK, AMPK, and β-actin. *B*) [^{3}H]Serine-labeled hepatocytes from SphK1$^{+/+}$ or SphK1$^{-/-}$ mice were infected with Ad5GFP or Ad5ASM. Radiolabeled S1P was measured (left panels). Primary cultured rat hepatocytes were treated with or without S1P (1 μM) for 8 h (middle top panel). Primary cultured rat hepatocytes were infected with Ad5GFP or adenovirus expressing human neutral ceramidase (Ad5NCD) (middle bottom panel). Protein extracts from the hepatocytes were subjected to immunoblot for p-AKT, p-AMPK, and β-actin. *C*) Primary cultured rat hepatocytes were infected with Ad5GFP or Ad5ASM (10 PFU/cell), and incubated for 2 h. Then, cells were treated with or without the indicated concentration of PTX for 24 h. Top panel: protein extracts from hepatocytes were subjected to immunoblot for p-AKT and AKT. Relative densitometric intensity of p-AKT and p-AMPK was determined for each protein band of the sample and normalized to AKT and AMPK, respectively (*A*, *B*, right panels; *C*, bottom panel). Results shown are representative of ≥3 independent experiments. Data are means ± SD from ≥4 independent experiments. $^*P < 0.05$.

cytes. In contrast, ASM deficiency inhibits glucose uptake, glycogen deposition, and lipid accumulation, resulting in glucose intolerance. In ASM$^{-/-}$ mice, similar levels of GSK3β phosphorylation were induced by food intake, whereas GLUT2 induction was reduced in comparison to the livers of ASM$^{+/+}$ mice (**Fig. 9*A***). Reduction of AMPK phosphorylation and induction of GLUT2 by high-dose glucose were inhibited in ASM$^{-/-}$ hepatocytes (Fig. 9*B*), whereas high-dose glucose did not affect AKT phosphorylation (data not shown). These results suggest that glu-

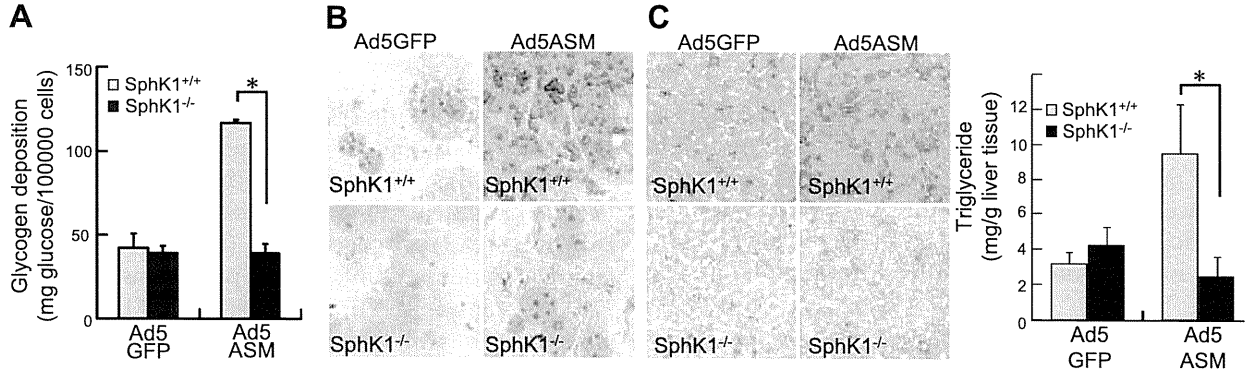

Figure 6. ASM-induced glycogen deposition and lipid accumulation are suppressed in SphK1$^{-/-}$ hepatocytes. *A*) Primary cultured hepatocytes isolated from SphK1$^{+/+}$ or SphK1$^{-/-}$ mice were infected with Ad5GFP or Ad5ASM. Glycogen content in hepatocytes was determined. *B*) Lipid droplets in SphK1$^{+/+}$or SphK1$^{-/-}$ hepatocytes infected with Ad5GFP or Ad5ASM were assessed by Oil Red O staining (original view ×800). *C*) SphK1$^{+/+}$ or SphK1$^{-/-}$ mice were infected with Ad5GFP or Ad5ASM, followed by assessment for hepatic lipid content by Oil Red O staining (left panel; original view ×200) and triglyceride measurement (right panel) in food-deprivation conditions at 7 d after the infection (original view ×200). Results shown are representative of ≥3 independent experiments. Data are means ± SD from ≥4 independent experiments. $^*P < 0.05$.

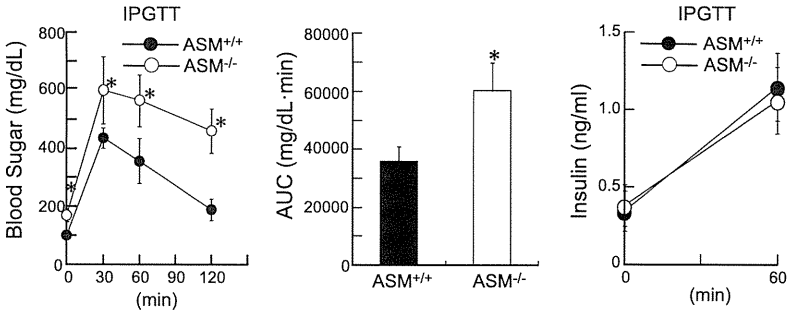

Figure 7. $ASM^{-/-}$ mice were glucose intolerant. *A*) $ASM^{+/+}$ and $ASM^{-/-}$ mice were deprived of food for 18 h, and IPGTT was performed by administering a glucose load of 2 mg/g body weight. Serial glucose (left panel) and insulin (right panel) were measured at the indicated time points. Blood glucose values for area under the curve (AUC) were calculated (middle panel). Results shown are representative of ≥3 independent experiments. Data are means ± SD from ≥4 independent experiments. $^*P < 0.05$.

cose intolerance in $ASM^{-/-}$ mice was due, at least in part, to insufficient reduction of AMPK activity and induction of GLUT2.

DISCUSSION

The present study addresses the contributions of ASM to glucose and lipid metabolism in the liver. The sphingomyelin/ceramide/S1P pathway is involved in glucose metabolism (6–9, 12–14, 21). Food intake reduced most sphingomyelin species in the mouse liver (Supplemental Table S2). Likewise, high-dose glucose reduced sphingomyelin species in primary cultured hepatocytes (Supplemental Table S2), suggesting that this pathway is related to glucose metabolism in hepatocytes. In our study using hepatocytes, ASM induced insulin-like effects such as glucose uptake, glycogen deposition, and lipid accumulation *via* S1P-mediated AKT activation. Ceramide attenuates insulin signaling, including AKT activation (14–16), thereby contributing to insulin resistance through multiple pathways (13, 15). In primary cultured hepatocytes, the effect of ASM introduction on ceramide level was smaller than that in sphingomyelin degradation, suggesting that the generated ceramide is further converted to S1P. Ceramide and S1P often exert opposing effects; thus, the balance between these two sphingolipids may be important for AKT activation. During ASM activation, the balance is inclined toward S1P, resulting in AKT activation. Indeed, ASM did not activate AKT in $SphK1^{-/-}$ hepatocytes, suggesting that ASM mediates insulin-like effects *via* S1P formation. S1P acts as a ligand for the S1PRs and also as an intracellular second messenger (31, 32). Among S1PRs, G_i-associated S1PR1 (33) is mainly expressed in the liver (34), and PTX pretreatment inhibited exogenous S1P-induced AKT phosphorylation in

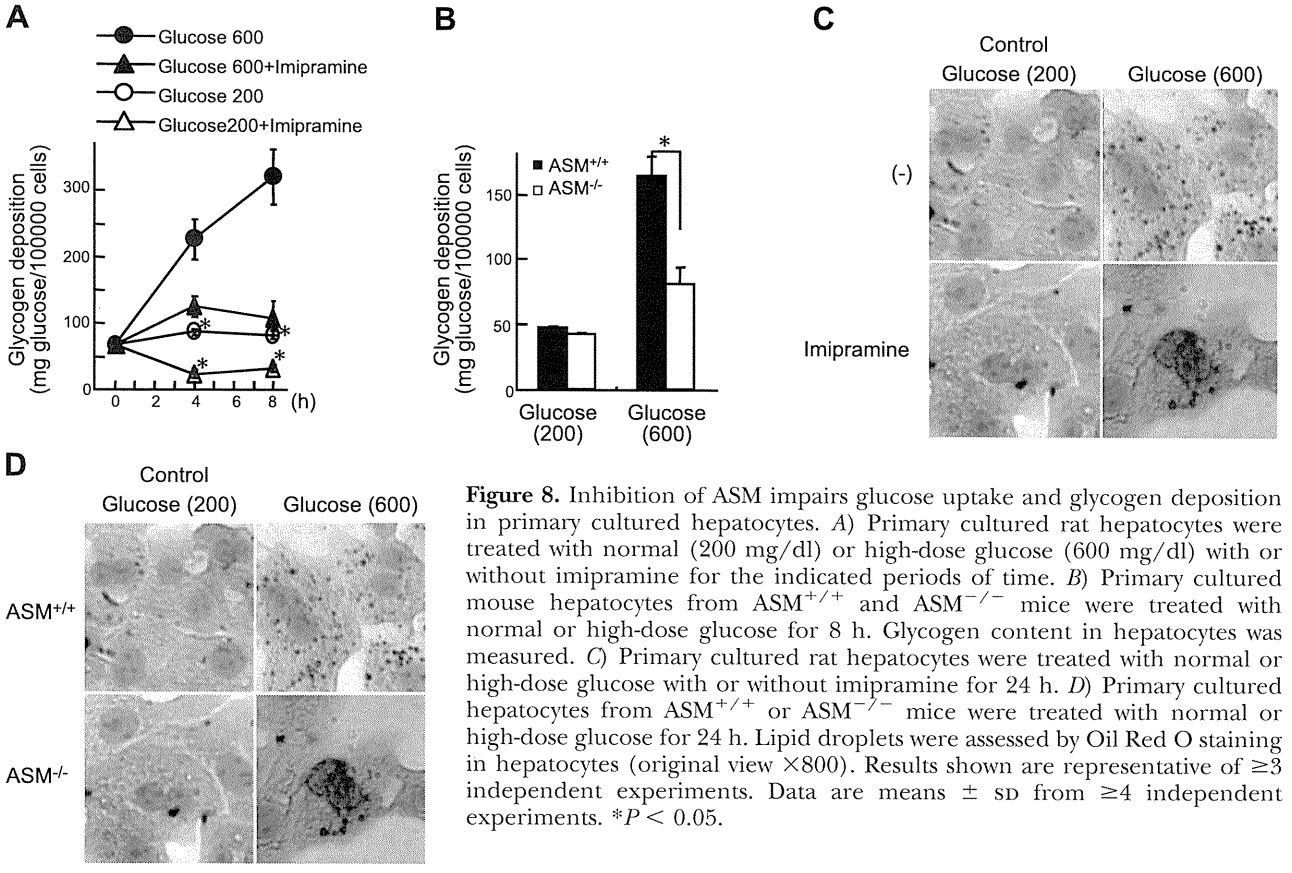

Figure 8. Inhibition of ASM impairs glucose uptake and glycogen deposition in primary cultured hepatocytes. *A*) Primary cultured rat hepatocytes were treated with normal (200 mg/dl) or high-dose glucose (600 mg/dl) with or without imipramine for the indicated periods of time. *B*) Primary cultured mouse hepatocytes from $ASM^{+/+}$ and $ASM^{-/-}$ mice were treated with normal or high-dose glucose for 8 h. Glycogen content in hepatocytes was measured. *C*) Primary cultured rat hepatocytes were treated with normal or high-dose glucose with or without imipramine for 24 h. *D*) Primary cultured hepatocytes from $ASM^{+/+}$ or $ASM^{-/-}$ mice were treated with normal or high-dose glucose for 24 h. Lipid droplets were assessed by Oil Red O staining in hepatocytes (original view ×800). Results shown are representative of ≥3 independent experiments. Data are means ± SD from ≥4 independent experiments. $^*P < 0.05$.

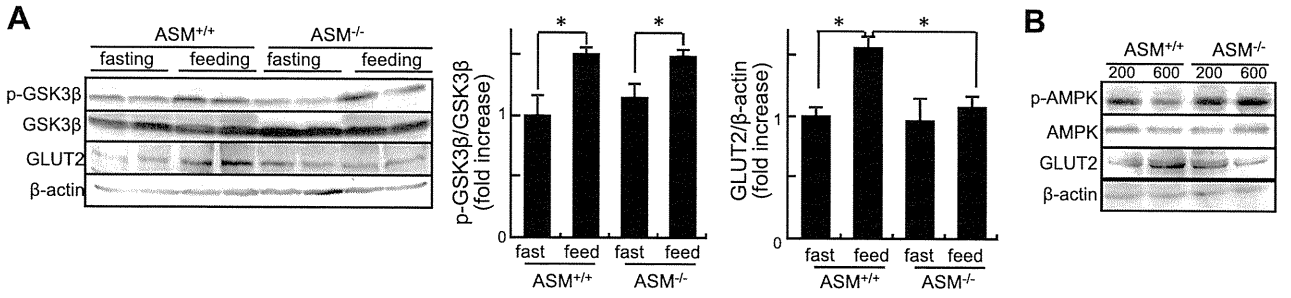

Figure 9. Inhibition of ASM suppresses GLUT2 induction. *A*) $ASM^{+/+}$ and $ASM^{-/-}$ mice were killed in both nonfeeding (fasting; 18 h food deprivation) and feeding conditions. Protein extracts from liver tissue were subjected to immunoblot for phosphorylated (p)-GSK3β, GSK3β, GLUT2, and β-actin (left panel). Relative densitometric intensity of p-GSK3β (middle panel) and GLUT2 (right panel) was determined for each protein band of the liver tissue sample and normalized to GSK3β and β-actin, respectively. *B*) Primary cultured hepatocytes from $ASM^{+/+}$ and $ASM^{-/-}$ mice were treated with normal (200 mg/dl) or high-dose glucose (600 mg/dl) for 8 h. Protein extracts from hepatocytes were subjected to immunoblot for p-AMPK, AMPK, GLUT2, and β-actin. Results shown are representative of ≥3 independent experiments. $*P < 0.05$.

primary cultured hepatocytes (data not shown), suggesting that S1P may activate AKT through predominantly S1PR1. PTX treatment partially inhibits ASM-induced AKT activation, suggesting that the generated S1P activates AKT at least partially *via* S1PRs and may also activate AKT through receptor-independent mechanisms.

In addition to AKT, AMPK also contributes to glucose metabolism. AMPK is a serine/threonine protein kinase that senses the immediate availability of cellular energy. Activated AMPK switches on catabolic pathways and switches off protein, carbohydrate, and lipid biosynthesis (anabolic pathways; ref. 35). Activation of AMPK in the liver reduces glycogen synthesis and lipogenesis as well as expression of GLUT2 (3). Activation of AMPK by 5-amino-4-imidazolecarboxamide riboside diminishes GLUT2 expression in primary cultured hepatocytes (36). Indeed, DN-AMPK increased glycogen deposition and lipid accumulation in primary hepatocytes and HepG2 cells (data not shown and ref. 37). Thus, in addition to increased AKT activation, reduced AMPK activation may be associated with another anabolic effect of ASM. Ceramide decreases (38) but S1P increases (39) AMPK phosphorylation in endothelial cells. In our study, ASM-induced AMPK inhibition in hepatocytes was independent of S1P. Thus, the decrease in AMPK activity may be due to ceramide processed by ASM.

Ad5ASM-infected mice showed improved glucose tolerance. Because adenovirus preferentially infects hepatocytes, the decrease in blood glucose was due to a variation of hepatic glucose metabolism, although sphingolipids have roles in glucose metabolism in muscle (40) and adipocytes (6–8). The ASM-induced decrease in blood glucose may be attributed to increased uptake of hepatic glucose rather than decreased production, because introduction of ASM did not affect the activity of adenylate cyclase, the glucagon target enzyme, in primary cultured rat hepatocytes (data not shown). The effects of ASM on hepatocytes are comparable to those of insulin. However, the introduction of hepatic ASM improved hyperglycemia in *db/db* mice with type 2 diabetes without increasing insulin levels (data not shown), indicating that ASM may reduce blood glucose regardless of the presence of insulin resistance. Instead of decreasing blood glucose, ASM increased hepatic triglyceride content, suggesting that ASM stimulates lipogenesis, in which transported glucose is converted to triacylglycerol (41). The effects of exogenous ASM in the liver are similar to the effects of deletion of hepatic phosphatase and tension homolog on chromosome 10 (PTEN), which is a negative regulator of AKT. Deletion of PTEN in the liver results in hyperphosphorylation of hepatic AKT and improves glucose tolerance but induces fatty liver in mice (42).

$ASM^{-/-}$ mice are glucose intolerant. The abnormality is not due to inactivation of the AKT/GSK3β pathway but is due, in part, to insufficient reduction of AMPK activity and induction of GLUT2. In addition, crosstalk may occur between ASM and various signaling pathways, including those of glucose and lipid metabolism, because ASM regulates sphingolipids in lipid raft microdomains that function as platforms for signal transduction and protein sorting (18). For example, disruption of lipid raft microdomains or chronic ethanol exposure inhibits localization of TC10 to lipid rafts,

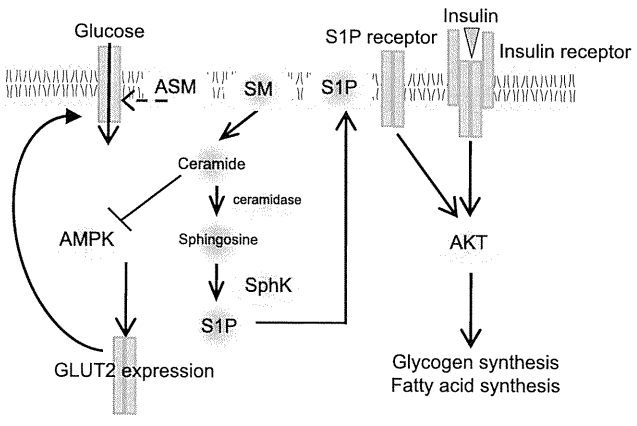

Figure 10. Hypothetical signals induced by ASM. Acid sphingomyelinase regulates glucose and lipid metabolism through AKT activation and AMPK suppression in hepatocytes. AKT activation is induced through S1P formation. AMPK suppression increases GLUT2 expression.

which induces GLUT4 translocation and glucose intake without affecting phosphatidylinositol-3 kinase/AKT signaling in adipocytes (43, 44). Pretreatment with imipramine inhibited high-dose glucose-induced lipid accumulation in rat hepatocytes, as did the knockout of ASM in mouse hepatocytes. As reported previously, the ASM inhibitor desipramine attenuates triglyceride increase by high-dose palmitic acid treatment in HepG2 cells (9). Moreover, a high-fat, high-cholesterol diet does not induce hepatic triacylglyceride accumulation in $ASM^{-/-}$ mice under LDL receptor-deficient conditions (9). These observations further support the role of ASM as a regulator of triglyceride synthesis in addition to glucose uptake. Further studies will determine the precise mechanism underlying the anabolic effects of ASM and its activation and ceramide/S1P regulation (45). The hypothetical roles of ASM are schematically summarized in **Fig. 10**.

In conclusion, overexpression of ASM in the liver improves glucose tolerance in both wild-type and diabetic *db/db* mice. ASM stimulates glucose uptake, glycogen deposition, and lipid accumulation in hepatocytes *via* AKT and GSK3β phosphorylation, which requires S1P formation. In addition, ASM decreases AMPK phosphorylation through ceramides, leading to GLUT2 up-regulation. Indeed, inactivation of ASM produces glucose intolerance in hepatocytes. Targeting ASM may become a new therapeutic strategy in type 2 diabetes. FJ

The authors thank Dr. Jacek Bielawski (Medical University of South Carolina, Charleston, SC, USA) for sphingolipid measurement, Dr. Yoko Sugiyama (Gifu University Graduate School of Medicine, Gifu, Japan) for measurement of adenylate cyclase activity, and Dr. Kenneth Walsh (Boston University, Boston, MA, USA) for adenoviruses encoding CA-AMPK and DN-AMPK. This work was supported by grants from Mitsubishi Pharma Research Foundation and the Ministry of Education, Culture, Sports, Science, and Technology of Japan (19790478 and 21790657 to Y.O. and 21390179 to M.S.).

REFERENCES

1. Thorens, B., Sarkar, H. K., Kaback, H. R., and Lodish, H. F. (1988) Cloning and functional expression in bacteria of a novel glucose transporter present in liver, intestine, kidney, and β-pancreatic islet cells. *Cell* **55,** 281–290
2. Rencurel, F., Waeber, G., Antoine, B., Rocchiccioli, F., Maulard, P., Girard, J., and Leturque, A. (1996) Requirement of glucose metabolism for regulation of glucose transporter type 2 (GLUT2) gene expression in liver. *Biochem. J.* **314**(Pt. 3), 903–909
3. Foretz, M., Ancellin, N., Andreelli, F., Saintillan, Y., Grondin, P., Kahn, A., Thorens, B., Vaulont, S., and Viollet, B. (2005) Short-term overexpression of a constitutively active form of AMP-activated protein kinase in the liver leads to mild hypoglycemia and fatty liver. *Diabetes* **54,** 1331–1339
4. Smith, E. L., and Schuchman, E. H. (2008) The unexpected role of acid sphingomyelinase in cell death and the pathophysiology of common diseases. *FASEB J.* **22,** 3419–3431
5. Gorska, M., Baranczuk, E., and Dobrzyn, A. (2003) Secretory Zn2+-dependent sphingomyelinase activity in the serum of patients with type 2 diabetes is elevated. *Horm. Metab. Res.* **35,** 506–507
6. Liu, P., Leffler, B. J., Weeks, L. K., Chen, G., Bouchard, C. M., Strawbridge, A. B., and Elmendorf, J. S. (2004) Sphingomyelinase activates GLUT4 translocation via a cholesterol-dependent mechanism. *Am. J. Physiol. Cell Physiol.* **286,** C317–C329
7. David, T. S., Ortiz, P. A., Smith, T. R., and Turinsky, J. (1998) Sphingomyelinase has an insulin-like effect on glucose transporter translocation in adipocytes. *Am. J. Physiol.* **274,** R1446–1453
8. Al-Makdissy, N., Younsi, M., Pierre, S., Ziegler, O., and Donner, M. (2003) Sphingomyelin/cholesterol ratio: an important determinant of glucose transport mediated by GLUT-1 in 3T3–L1 preadipocytes. *Cell. Signal.* **15,** 1019–1030
9. Deevska, G. M., Rozenova, K. A., Giltiay, N. V., Chambers, M. A., White, J., Boyanovsky, B. B., Wei, J., Daugherty, A., Smart, E. J., Reid, M. B., Merrill, A. H., Jr., and Nikolova-Karakashian, M. (2009) Acid sphingomyelinase deficiency prevents diet-induced hepatic triacylglycerol accumulation and hyperglycemia in mice. *J. Biol. Chem.* **284,** 8359–8368
10. Jenkins, R. W., Canals, D., and Hannun, Y. A. (2009) Roles and regulation of secretory and lysosomal acid sphingomyelinase. *Cell. Signal.* **21,** 836–846
11. Hannun, Y. A. (1996) Functions of ceramide in coordinating cellular responses to stress. *Science* **274,** 1855–1859
12. Summers, S. A., and Nelson, D. H. (2005) A role for sphingolipids in producing the common features of type 2 diabetes, metabolic syndrome X, and Cushing's syndrome. *Diabetes* **54,** 591–602
13. Holland, W. L., Brozinick, J. T., Wang, L. P., Hawkins, E. D., Sargent, K. M., Liu, Y., Narra, K., Hoehn, K. L., Knotts, T. A., Siesky, A., Nelson, D. H., Karathanasis, S. K., Fontenot, G. K., Birnbaum, M. J., and Summers, S. A. (2007) Inhibition of ceramide synthesis ameliorates glucocorticoid-, saturated-fat-, and obesity-induced insulin resistance. *Cell Metab.* **5,** 167–179
14. Holland, W. L., and Summers, S. A. (2008) Sphingolipids, insulin resistance, and metabolic disease: new insights from in vivo manipulation of sphingolipid metabolism. *Endocr. Rev.* **29,** 381–402
15. Wymann, M. P., and Schneiter, R. (2008) Lipid signalling in disease. *Nat. Rev. Mol. Cell Biol.* **9,** 162–176
16. Stratford, S., DeWald, D. B., and Summers, S. A. (2001) Ceramide dissociates 3′-phosphoinositide production from pleckstrin homology domain translocation. *Biochem. J.* **354,** 359–368
17. Liangpunsakul, S., Sozio, M. S., Shin, E., Zhao, Z., Xu, Y., Ross, R. A., Zeng, Y., and Crabb, D. W. Inhibitory effect of ethanol on AMPK phosphorylation is mediated in part through elevated ceramide levels. *Am. J. Physiol. Gastrointest. Liver Physiol.* **298,** G1004–G1012
18. Tani, M., Ito, M., and Igarashi, Y. (2007) Ceramide/sphingosine/sphingosine 1-phosphate metabolism on the cell surface and in the extracellular space. *Cell. Signal.* **19,** 229–237
19. Osawa, Y., Banno, Y., Nagaki, M., Brenner, D. A., Naiki, T., Nozawa, Y., Nakashima, S., and Moriwaki, H. (2001) TNF-α-induced sphingosine 1-phosphate inhibits apoptosis through a phosphatidylinositol 3-kinase/Akt pathway in human hepatocytes. *J. Immunol.* **167,** 173–180
20. Osawa, Y., Uchinami, H., Bielawski, J., Schwabe, R. F., Hannun, Y. A., and Brenner, D. A. (2005) Roles for C16-ceramide and sphingosine 1-phosphate in regulating hepatocyte apoptosis in response to tumor necrosis factor-α. *J. Biol. Chem.* **280,** 27879–27887
21. Rapizzi, E., Taddei, M. L., Fiaschi, T., Donati, C., Bruni, P., and Chiarugi, P. (2009) Sphingosine 1-phosphate increases glucose uptake through trans-activation of insulin receptor. *Cell. Mol. Life Sci.* **66,** 3207–3218
22. Osawa, Y., Hannun, Y. A., Proia, R. L., and Brenner, D. A. (2005) Roles of AKT and sphingosine kinase in the antiapoptotic effects of bile duct ligation in mouse liver. *Hepatology* **42,** 1320–1328
23. Allende, M. L., Sasaki, T., Kawai, H., Olivera, A., Mi, Y., van Echten-Deckert, G., Hajdu, R., Rosenbach, M., Keohane, C. A., Mandala, S., Spiegel, S., and Proia, R. L. (2004) Mice deficient in sphingosine kinase 1 are rendered lymphopenic by FTY720. *J. Biol. Chem.* **279,** 52487–52492
24. Adachi, M., and Brenner, D. A. (2008) High molecular weight adiponectin inhibits proliferation of hepatic stellate cells via activation of adenosine monophosphate-activated protein kinase. *Hepatology* **47,** 677–685

25. Bligh, E.G., and Dyer, W. J. (1959) A rapid method of total lipid extraction and purification. *Can. J. Biochem. Physiol.* **37,** 911–917
26. Pettus, B. J., Bielawski, J., Porcelli, A. M., Reames, D. L., Johnson, K. R., Morrow, J., Chalfant, C. E., Obeid, L. M., and Hannun, Y. A. (2003) The sphingosine kinase 1/sphingosine-1-phosphate pathway mediates COX-2 induction and PGE_2 production in response to TNF-α. *FASEB J.* **17,** 1411–1421
27. Gonzalez, A. A., Kumar, R., Mulligan, J. D., Davis, A. J., Weindruch, R., and Saupe, K. W. (2004) Metabolic adaptations to fasting and chronic caloric restriction in heart, muscle, and liver do not include changes in AMPK activity. *Am. J. Physiol. Endocrinol. Metab.* **287,** E1032–E1037
28. Wojtaszewski, J. F., Jorgensen, S. B., Hellsten, Y., Hardie, D. G., and Richter, E. A. (2002) Glycogen-dependent effects of 5-aminoimidazole-4-carboxamide (AICA)-riboside on AMP-activated protein kinase and glycogen synthase activities in rat skeletal muscle. *Diabetes* **51,** 284–292
29. Zang, M., Zuccollo, A., Hou, X., Nagata, D., Walsh, K., Herscovitz, H., Brecher, P., Ruderman, N. B., and Cohen, R. A. (2004) AMP-activated protein kinase is required for the lipid-lowering effect of metformin in insulin-resistant human HepG2 cells. *J. Biol. Chem.* **279,** 47898–47905
30. Grassme, H., Gulbins, E., Brenner, B., Ferlinz, K., Sandhoff, K., Harzer, K., Lang, F., and Meyer, T. F. (1997) Acidic sphingomyelinase mediates entry of *N. gonorrhoeae* into nonphagocytic cells. *Cell* **91,** 605–615
31. Pyne, S., and Pyne, N. J. (2002) Sphingosine 1-phosphate signalling and termination at lipid phosphate receptors. *Biochim. Biophys. Acta* **1582,** 121–131
32. Olivera, A., and Spiegel, S. (1993) Sphingosine-1-phosphate as second messenger in cell proliferation induced by PDGF and FCS mitogens. *Nature* **365,** 557–560
33. Siehler, S., and Manning, D. R. (2002) Pathways of transduction engaged by sphingosine 1-phosphate through G protein-coupled receptors. *Biochim. Biophys. Acta* **1582,** 94–99
34. Yang, A. H., Ishii, I., and Chun, J. (2002) In vivo roles of lysophospholipid receptors revealed by gene targeting studies in mice. *Biochim. Biophys. Acta* **1582,** 197–203
35. Hardie, D. G. (2007) AMP-activated/SNF1 protein kinases: conserved guardians of cellular energy. *Nat. Rev. Mol. Cell Biol.* **8,** 774–785
36. Leclerc, I., Lenzner, C., Gourdon, L., Vaulont, S., Kahn, A., and Viollet, B. (2001) Hepatocyte nuclear factor-4α involved in type 1 maturity-onset diabetes of the young is a novel target of AMP-activated protein kinase. *Diabetes* **50,** 1515–1521
37. Hou, X., Xu, S., Maitland-Toolan, K. A., Sato, K., Jiang, B., Ido, Y., Lan, F., Walsh, K., Wierzbicki, M., Verbeuren, T. J., Cohen, R. A., and Zang, M. (2008) SIRT1 regulates hepatocyte lipid metabolism through activating AMP-activated protein kinase. *J. Biol. Chem.* **283,** 20015–20026
38. Wu, Y., Song, P., Xu, J., Zhang, M., and Zou, M. H. (2007) Activation of protein phosphatase 2A by palmitate inhibits AMP-activated protein kinase. *J. Biol. Chem.* **282,** 9777–9788
39. Igarashi, J., Shoji, K., Hashimoto, T., Moriue, T., Yoneda, K., Takamura, T., Yamashita, T., Kubota, Y., and Kosaka, H. (2009) Transforming growth factor-β1 down-regulates caveolin-1 expression and enhances sphingosine 1-phosphate signaling in cultured vascular endothelial cells. *Am. J. Physiol. Cell Physiol* **297,** C1263–C1274
40. Adams, J. M., 2nd, Pratipanawatr, T., Berria, R., Wang, E., DeFronzo, R. A., Sullards, M. C., and Mandarino, L. J. (2004) Ceramide content is increased in skeletal muscle from obese insulin-resistant humans. *Diabetes* **53,** 25–31
41. Glimcher, L. H., and Lee, A. H. (2009) From sugar to fat: How the transcription factor XBP1 regulates hepatic lipogenesis. *Ann. N. Y. Acad. Sci.* **1173**(Suppl. 1), E2–E9
42. Stiles, B., Wang, Y., Stahl, A., Bassilian, S., Lee, W. P., Kim, Y.-J., Sherwin, R., Devaskar, S., Lesche, R., Magnuson, M. A., and Wu, H. (2004) Live-specific deletion of negative regulator Pten results in fatty liver and insulin hypersensitivity. *Proc. Natl. Acad. Sci. U. S. A.* **101,** 2082–2087
43. Watson, R. T., Shigematsu, S., Chiang, S. H., Mora, S., Kanzaki, M., Macara, I. G., Saltiel, A. R., and Pessin, J. E. (2001) Lipid raft microdomain compartmentalization of TC10 is required for insulin signaling and GLUT4 translocation. *J. Cell Biol.* **154,** 829–840
44. Sebastian, B. M., and Nagy, L. E. (2005) Decreased insulin-dependent glucose transport by chronic ethanol feeding is associated with dysregulation of the Cbl/TC10 pathway in rat adipocytes. *Am. J. Physiol. Endocrinol. Metab.* **289,** E1077–E1084
45. Zeidan, Y. H., and Hannun, Y. A. (2010) The acid sphingomyelinase/ceramide pathway: biomedical significance and mechanisms of regulation. *Curr. Mol. Med.* **10,** 454–466

Received for publication July 23, 2010.
Accepted for publication December 2, 2010.